communications biology

Article

https://doi.org/10.1038/s42003-024-07100-w

Two ubiquitous aldo-keto reductases in the genus *Papaver* support a patchwork model for morphine pathway evolution

Check for updates

Samuel C. Carr[1,3], Fasih Rehman[1], Jillian M. Hagel[1,4], Xue Chen[1], Kenneth K. S. Ng[2] & Peter J. Facchini[1]

The evolution of morphinan alkaloid biosynthesis in plants of the genus *Papaver* includes permutation of several processes including gene duplication, fusion, neofunctionalization, and deletion resulting in the present chemotaxonomy. A critical gene fusion event resulting in the key bifunctional enzyme reticuline epimerase (REPI), which catalyzes the stereochemical inversion of (*S*)-reticuline, was suggested to precede neofunctionalization of downstream enzymes leading to morphine biosynthesis in opium poppy (*Papaver somniferum*). The ancestrally related aldo-keto reductases 1,2-dehydroreticuline reductase (DRR), which occurs in some species as a component of REPI, and codeinone reductase (COR) catalyze the second and penultimate steps, respectively, in the pathway converting (*S*)-reticuline to morphine. Orthologs for each enzyme isolated from the transcriptomes of 12 *Papaver* species were shown to catalyze their respective reactions in species that capture states of the metabolic pathway prior to key evolutionary events, including the gene fusion event leading to REPI, thus suggesting a patchwork model for pathway evolution. Analysis of the structure and substrate preferences of DRR orthologs in comparison with COR orthologs revealed structure-function relationships underpinning the functional latency of DRR and COR orthologs in the genus *Papaver*, thus providing insights into the molecular events leading to the evolution of the pathway.

Benzylisoquinoline alkaloids (BIAs) comprise a large family of structurally and functionally diverse plant specialized metabolites found primarily in the order *Ranunculales*[1]. BIAs exhibit potent pharmacological properties and include the vasodilator papaverine, the tumor suppressant and antitussive agent noscapine, the analgesics morphine and codeine, and semisynthetic derivatives of thebaine, such as oxycodone and the opioid antagonist naloxone[2]. Opium poppy (*Papaver somniferum*) as a cultivated crop remains the sole commercial source of all pharmaceutical opiates[3], and is the only plant known to produce morphine and codeine, although other *Papaver* species accumulate the morphinan pathway intermediate thebaine.

The first committed step in morphinan alkaloid biosynthesis is the stereochemical inversion of the central branchpoint intermediate, (*S*)-reticuline[1], from which most BIAs are derived. The inversion is a result of carbon-carbon and carbon-oxygen mediated ring formation and rearrangement. In opium poppy, (*S*)-reticuline is converted to (*R*)-reticuline by a unique fusion protein, reticuline epimerase (REPI), consisting of a translational coupling between a cytochrome P450 (CYP) and an aldo-keto reductase (AKR)[4,5]. Eight additional enzymes convert (*R*)-reticuline to morphine (Fig. 1A), including another CYP[4–6], AKR[4,5,7], one short chain dehydrogenase (SDR)[8], two pathogenesis-related 10 proteins (PR10s)[9,10], two Fe^{2+}/2-oxoglutarate-dependent dioxygenases (DIOXs)[11], and one acetyl-CoA-dependent acyltransferase (AT)[12]. The repeated recruitment of functionally distinct enzymes belonging to a limited number of protein families is a common theme in BIA metabolism. Recently, whole genome sequencing and comparative transcriptome analyzes, coupled with targeted alkaloid profiling, have begun to reveal key evolutionary events that have shaped BIA biosynthesis across members of the genus *Papaver*. Current models predict a dynamic evolutionary process whereby gene duplication, clustering, fusion, and deletion events have contributed to the recruitment and neofunctionalization of new biosynthetic enzymes, which ultimately facilitated the production of morphinan alkaloids in some *Papaver* species and, more specifically, the unique occurrence of morphine in opium poppy[13–16].

[1]Department of Biological Sciences, University of Calgary, Calgary, AB, Canada. [2]Department of Chemistry and Biochemistry, University of Windsor, Windsor, ON, Canada. [3]Present address: Department of Natural Product Biosynthesis, Max Planck Institute for Chemical Ecology, Jena, Germany. [4]Present address: Enveric Biosciences Inc., Calgary, AB, Canada. e-mail: pfacchin@ucalgary.ca

A patchwork model of metabolic pathway evolution[17,18], which has been proposed for morphine[14] and caffeine[19] biosynthesis among other plant specialized metabolites, predicts that the latent catalytic promiscuity of some metabolic enzymes can be co-opted into new biosynthetic pathways[20,21]. A background network of latent enzyme promiscuity, dubbed the 'underground metabolism'[22], provides a platform for the recruitment of

A

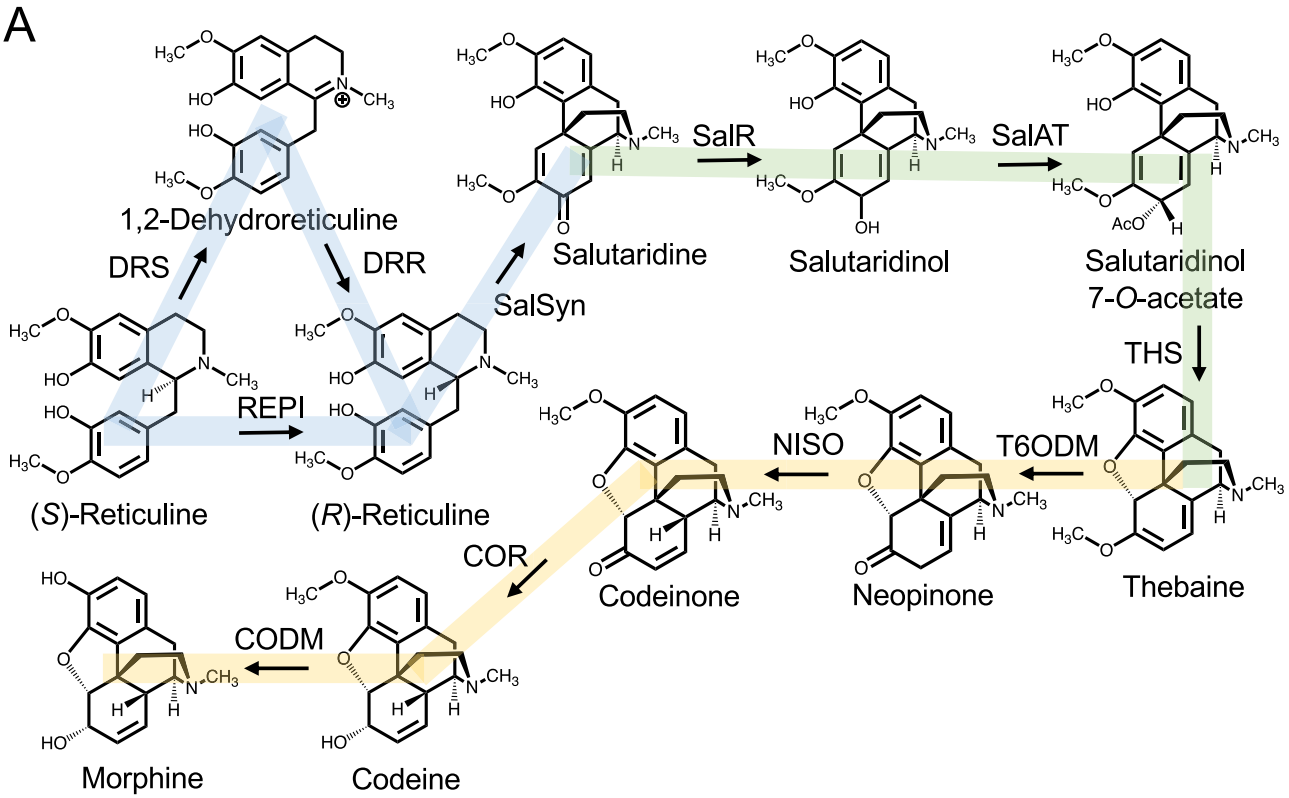

B

Papaver species	(*R*/*S*)-Reticuline	Salutaridine	Thebaine	Codeinone	Codeine	Morphine
somniferum	+	+	+	+	+	+
rhoeas	+	nd	nd	nd	nd	nd
glaucum	+	nd	nd	nd	nd	nd
*dubium**	nd	nd	nd	nd	nd	nd
*bracteatum**	+*	+*	+*	nd	nd	nd
lasiothrix	+	+*	+*	nd	nd	nd
orientale	+	+	+*	nd	nd	nd
*armeniacum**	+*	+*	nd	nd	nd	nd
triniifolium	+	+	nd	nd	nd	nd
spicatum	+	+	nd	nd	nd	nd
apokrinomenon	nd	nd	nd	nd	nd	nd
atlanticum	+	nd	nd	nd	nd	nd
rupifragium	+	nd	nd	nd	nd	nd
*californicum**	+*	nd	nd	nd	nd	nd
alpinum	+	nd	nd	nd	nd	nd
burseri	+	+	nd	nd	nd	nd
nudicale	nd	+	nd	nd	nd	nd
miyabeanum	+	nd	nd	nd	nd	nd
radicatum	+	nd	nd	nd	nd	nd
*pavonium**	nd	nd	nd	nd	nd	nd

Fig. 1 | Alkaloid profiling of various *Papaver* species. A Morphinan alkaloid biosynthetic pathway in opium poppy. Steps from (*S*)-reticuline to salutaridine are highlighted in blue, the pathway from salutaridine to thebaine is highlighted in green, and the conversion of thebaine to morphine is highlighted in yellow. **B** Alkaloids in the pathway from (*S*)-reticuline to morphine detected in various *Papaver* species. '+' indicates that the corresponding alkaloid was identified and the abbreviation 'nd' indicates that no alkaloid was detected. '+*' indicate detected alkaloids reported in other published work[15,30].

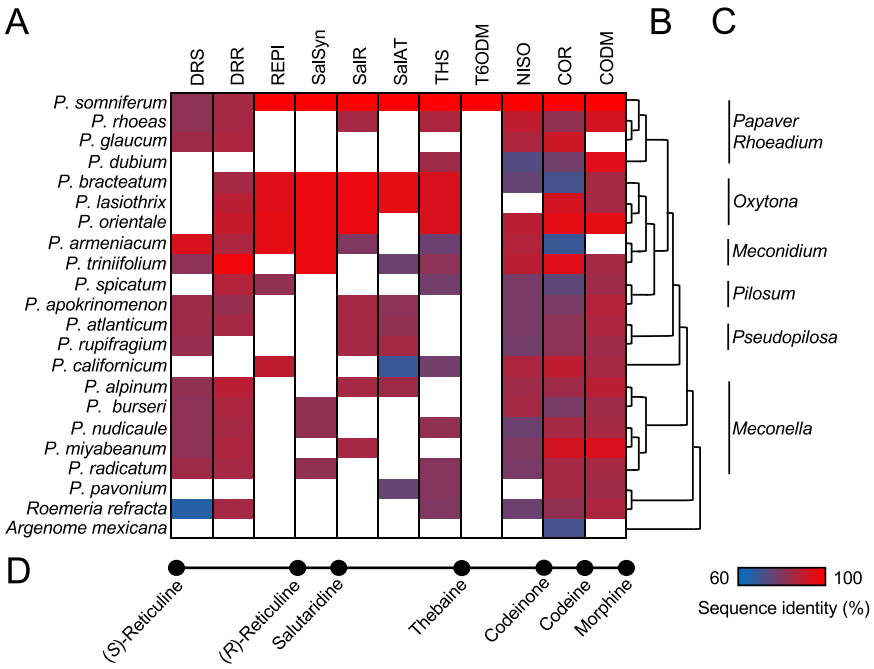

Fig. 2 | Transcript profiling of various *Papaver* species. A Occurrence of transcripts encoding proteins exhibiting greater than 60% amino acid sequence identity relative to enzymes involved in the conversion of (*S*)-reticuline to morphine in opium poppy. Nucleotide sequencing and contig assembly statistics are provided for each transcriptome in Table S8. Transcripts showing relatively higher predicted amino acid sequence identity with a different enzyme were omitted. Numerical percent identities and indication of partial and truncated transcript with the corresponding percent coverage are provided in Fig S2. Relative amino acid sequence identity with the corresponding opium poppy biosynthetic enzyme is shown as a gradient from red (100%) to blue (60%). White indicates that no transcript was annotated. Transcriptomes from previously published work were used for *Papaver rhoeas*[31,32], *P. dubium P. bracteatum P. orientale P. armeniacum P. californicum* and *P. pavonium*[15], *R. refracta*[34], and *A. mexicana*[33]. **B** Consensus phylogenetic relationship among *Papaver* species based on previous published work[15,80]. **C** Selected section denominations of *Papaver* species. **D** Simplified diagram of the morphine biosynthetic pathway showing key metabolites from Fig. 1B and their corresponding position in panel **A**.

novel biosynthetic pathways whereby blocks of consecutive latent enzymatic activities may be linked together by key neofunctionalization events. The patchwork mechanism provides an attractive alternative to recruitment models suggesting the involvement of a specific selective pressure for the emergence of each new biosynthetic step by reducing the actual number of selection events. Gene duplication, via whole genome or local repetition processes, provides new genetic material for neofunctionalization and selection without compromising the function of the original gene.

REPI is an example of gene sequential duplication, clustering and fusion, and its role as the gateway into morphinan biosynthesis has been the focus of several recent studies[14–16]. REPI is a fusion of the CYP, 1,2-dehydroreticuline synthase (DRS), and the AKR, 1,2-dehydroreticuline reductase (DRR). The two-domain enzyme converts (*S*)-reticuline to (*R*)-reticuline via a two-step process, starting with the oxidation of (*S*)-reticuline by DRS yielding the iminium ion, 1,2-dehydroreticuline, from which the carbon-nitrogen double bond is subsequently reduced by DRR to form (*R*)-reticuline[4,5]. Phenol coupling of (*R*)-reticuline by the stereoselective CYP, salutaridine synthase (SalSyn), yields the pro-morphinan alkaloid salutaridine[6]. The fusion of DRS and DRR into REPI has been proposed as a pivotal event in the evolution of morphinan alkaloid biosynthesis[15,16]. Of particular interest is the relationship between DRR and codeinone reductase (COR), which catalyzes the penultimate step in the formation of morphine by reducing the ketone in codeinone to an alcohol in codeine and is the only other known AKR involved in BIA metabolism[7]. The AKR superfamily occurs in all phyla and plays diverse biological roles in plants, including detoxification of reactive molecules, carbon assimilation, iron acquisition, and the biosynthesis of specialized metabolites[23], such as isoflavonoids[24] and tropane alkaloids[25]. AKRs reduce a variety of functional groups, typically carbonyls such as aldehydes, ketones and quinones, atypically steroid double bonds, and in the case of REPI/DRR iminium ion carbon-nitrogen double bonds[23,26]. AKRs canonically employ a 'push and pull' mechanism involving a central catalytic tyrosine, which protonates or deprotonates the substrate with the aid of a histidine or lysine and an aspartate, while NADP(H) donates or accepts a hydride[23]. Atypical AKR mechanisms have been demonstrated primarily in the AKR1D family of steroid 5B-reductases[27,28]. Sequence, structural, and mutagenesis studies have shown COR to possess the canonical AKR tetrad, whereas homology modeling of DRR has revealed novel substitutions indicative of an atypical AKR mechanism[29]. The occurrence of different catalytic mechanisms poses intriguing questions about the evolutionary divergence of *DRR* and *COR* genes, and the fusion of DRR and DRS to form REPI.

In this work, we explore the evolution of morphinan alkaloid biosynthesis with a focus on the AKR enzymes, DRR, COR and REPI, and a consideration of early steps in the pro-morphinan alkaloid pathway. Using transcriptomics, kinetic characterization, structural reasoning based on homology models and molecular docking, and heterologous expression in yeast, we show the ubiquitous occurrence of functional orthologs for both *DRR* and *COR* in members of the genus *Papaver*.

Results

Alkaloid profiling of *Papaver* species

Alkaloid profiling was performed on 12 *Papaver* species (Fig. S1) and combined with previously published data on the distribution of morphinan alkaloids (Fig. 1B; Table S1). Phylogenetic relationships assembled from previous work[8,15,30] are shown in Fig. 2B. Previously reported morphinan alkaloid profiles that mostly agree with data presented herein are available for 6 of the 12 analyzed *Papaver* species. The only notable discrepancies were (i) the empirical detection of salutaridine in *P. nudicaule*, which was previously reported not to accumulate pro-morphinan or morphinan alkaloids[15], and (ii) the lack of salutaridine and thebaine in *P. lasiothrix*, which have been previously reported in this species[30]. In the 20 *Papaver* species shown in Fig. 1B, (i) *P. armeniacum*, *P. triniifolium*, *P. spicatum*, *P. burseri*, and *P. nudicaule* all accumulated salutaridine, (ii) *P. bracteatum*, *P. lasiothrix*, and *P. orientale* accumulated thebaine, and (iii) only *P. somniferum* accumulated codeinone, codeine, and morphine. *P. orientale* has also been reported to accumulate oripavine[15], which is formed by the 3-*O*-demethylation of thebaine.

Transcriptome analysis of morphinan biosynthetic genes in *Papaver* species

Gene orthologs corresponding to putative pro-morphinan and morphinan alkaloid biosynthetic genes were detected (Figs. 2 and S2) by nucleotide BLAST analysis of the 12 transcriptomes sequenced and assembled herein, and previously reported libraries[15,31–34] using *P. somniferum* biosynthetic genes as queries (Table S2). BLAST hits were sorted based on nucleotide sequence identity compared with known opium poppy biosynthetic

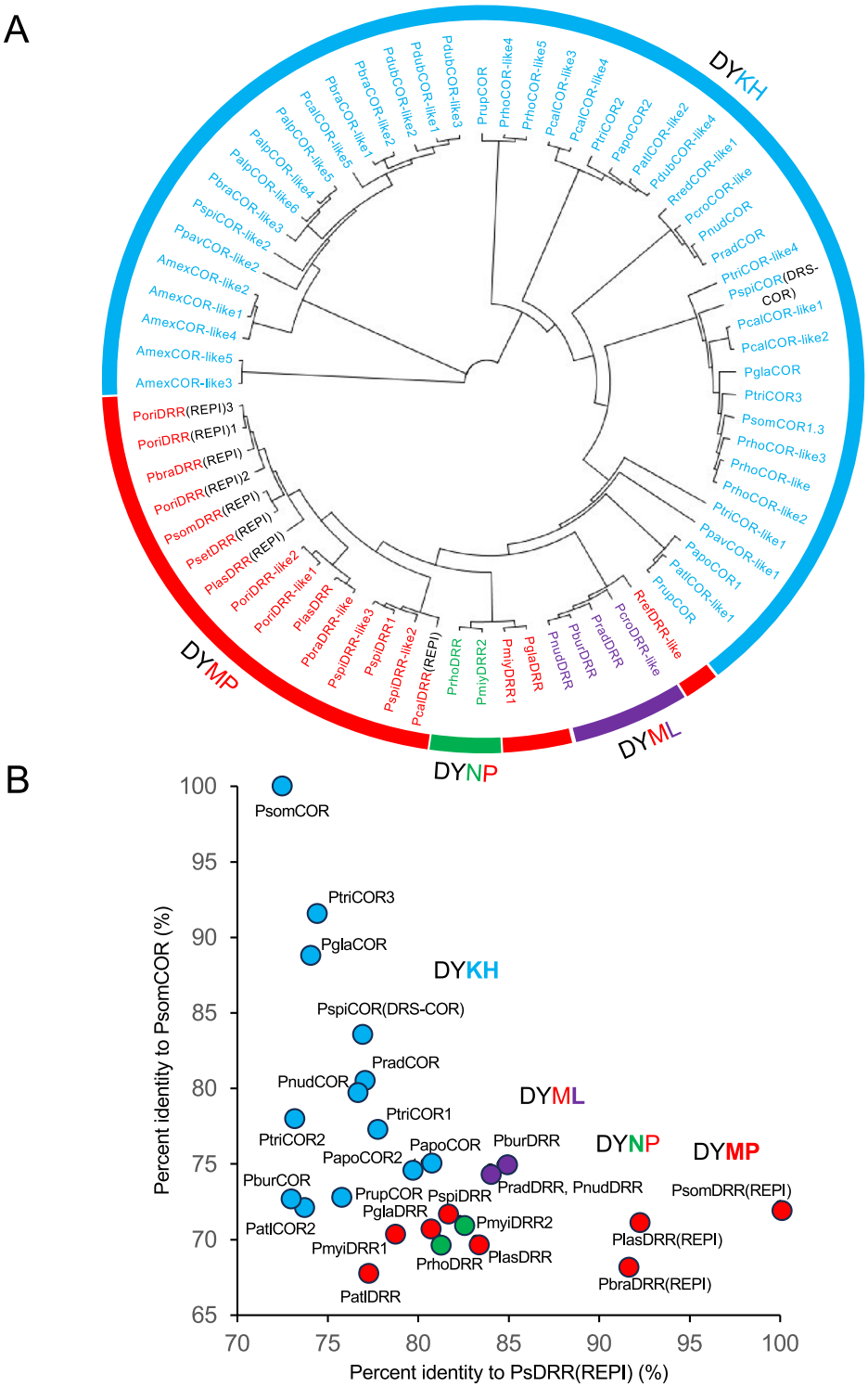

Fig. 3 | Phylogenetic and sequence similarity analysis of AKR homologs from various *Papaver* species. A Phylogenetic tree showing the relationships among full-length AKR transcripts found in transcriptomes from various *Papaver* species. Annotations of 'COR-like' or 'DRR-like' was based on the catalytic tetrad found in each predicted polypeptide. COR-like proteins containing the DYKH catalytic tetrad are shown in cyan, whereas DRR-like proteins are indicated in red (DYMP), purple (DYML), or green (DYNP). The function of transcripts lacking a 'like' suffix have been empirically confirmed. AKRs occurring as a fusion with a cytochrome P450 (i.e., a REPI homolog) are shown in black. The neighbor-joining tree was constructed using the Geneious tree-building Tamura-Nei model with a cost matrix of 65% similarity (5.0/−4.0), a gap open-penalty of 12, and a gap extension-penalty of 3 (nodes: 136; tips: 69). **B** Sequence similarity analysis of selected AKRs found in transcriptome from various *Papaver* species. Predicted proteins were plotted based on amino acid sequence identity compared with COR and DRR (from REPI), calculated using Clustal Omega[81]. COR-like proteins containing the DYKH catalytic tetrad are shown in cyan, whereas DRR-like proteins are indicated in red (DYMP), purple (DYML), or green (DYNP).

enzymes (Fig. S3) and omitted if a higher sequence identity to a different biosynthetic enzyme was observed. For species with available genomes (i.e., *P. bracteatum*, *P. armeniacum*, *P. atlanticum*, *P. californicum*, and *P. nudicaule*), transcripts were cross-referenced to genomic data for further validation (Fig. S4 and table S3). Orthologous gene families (orthogroups) were determined[35] to supplement BLAST analysis and investigate evolutionary relationships (Table S4).

The difficulty of accurately annotating transcripts based solely on sequence similarity is highlighted by several sets of enzyme families and subfamilies that share considerable amino acid sequence identity between pairs or within a group: AKR (i.e., DRR and COR), PR10 (i.e., THS and NISO), CYP719 [i.e., SalSyn and cheilanthifoline synthase (CheSyn)] and, in particular, DIOX (i.e., T6ODM, CODM, PODA, and DIOX6) family enzymes. A gradient of similarity across related enzymes precluded a trivial classification without functional characterization. AKR homologs of DRR and COR were initially classified based on catalytic tetrads whereby COR-like transcripts encoded proteins possessing the canonical AKR tetrad motif $D^{51}Y^{56}K^{86}H^{119}$ (COR numbering, abbreviated as DYKH), whereas DRR-like transcripts encoded proteins possessing the previously reported DYMP[29] and additional variants DYML and DYNP (Figs. 3 and S3E). No similar and clearly differentiating architectural features were found in other putative pro-morphinan or morphinan biosynthetic enzymes belonging to the PR10,

CYP719, SDR, AT, or DIOX families; thus, transcripts corresponding to these enzymes were annotated solely based on sequence identity. The CYP719s, SalSyn and CheSyn more clearly separated from each other (Fig. S3C). SalSyn was restricted to salutaridine-producing species; most distantly in the *Meconella P. burseri*, *P. radicatum*, and *P. miyabeanum*. *DIOX*-like transcripts were more ambiguous with all sequences sharing substantial identity with each other, which agrees with the reported substrate promiscuity of these enzymes[36]. *DIOX*-like transcripts were subcategorized as *CODM*-like, *PODA*-like, or *DIOX6*-like (Fig. S3A, B). Based on the criteria used, no DIOX-like transcripts were annotated as *T6ODM*-like. Although PODA-like transcripts from *P. rhoeas*, *P. triniifolium* and *P. miyabeanum* all shared >90% sequence identity with T6ODM, all three transcripts showed greater sequence identity with PODA (Fig. 3A, B). Interestingly, trace T6ODM activity has been observed in *P. somniferum* PODA[36]. Putative enzymes corresponding to PR10 proteins showed a gradient between THS- and NISO-like sequences (Fig. S3D). No closely related biosynthetic enzymes for other morphinan biosynthetic enzymes (i.e., DRS (CYP82Y2), SalR, and SalAT) were identified in these *Papaver* species.

The observed orthologous transcripts were consistent with the metabolite profiling for most *Papaver* species, with some key exceptions. Despite the occurrence of salutaridine, no transcripts corresponding to REPI were identified in *P. triniifolium, P. burseri, P. nudicaule*, and to a similar extant *P. spicatum*. However, transcripts with moderate to high sequence identity compared with the DRS and DRR moieties of *P. somniferum* REPI were detected, unfused (Fig. 2 and S2). In these species, unfused DRS and DRR may catalyze the conversion of (*S*)- to (*R*)-reticuline instead of REPI. An unusual DRS-COR fusion found in *P. spicatum* cannot be ruled out as a transcriptome assembly error, although this is unlikely. SalSyn transcripts were also missing in *P. spicatum* and SalAT in *P. orientale*; the latter having been previously reported[12]. Similar *DRS* and *DRR* pairs are found throughout the genus *Papaver*. Notably, unfused *DRS-DRR* pairs predicted to convert (*S*)-reticuline to (*R*)-reticuline in place of REPI are found in the more distantly related *Meconella* section before the earliest known instance of REPI in *P. californicum* (Figs. 2 and S2).

Pertinent to the concept of 'underground' metabolism, was the observation of orthologous transcripts in *Papaver* species lacking the associated pro-morphinan or morphinan alkaloids. Most striking, COR-like transcripts were found in all *Papaver* species, and detected in other members of the Papaveraceae including *R. refracta, Argemone mexicana*, *Chelidonium majus*[37], and *Corydalis yanhusuo*[38,39]. Transcripts from P. glaucum, *P. lasiothrix*, *P. orientale*, *P. triniifolium*, and most distantly *P. miyabeanum* shared over 90% sequence identity to *P. somniferum* COR. The roles of such COR-like transcripts are unknown since only *P. somniferum* accumulates the known COR substrates and products. DIOX-like transcripts with sequence identities closest to *P. somniferum* CODM were nearly ubiquitous across the *Papaver* genus and occurred even more broadly in other members of the Papaveraceae including *Roemeria refracta*. As mentioned above, the closely related DIOXs T6ODM, CODM, PODA, and DIOX6 preclude simple sequence-based assignment. Similar with COR-like transcripts, CODM, PODA, and DIOX6-like transcripts sharing over 90% sequence identity to their *P. somniferum* counterparts were found sporadically across the genus *Papaver*, most distantly in the *Meconella* section.

Papaver AKR orthologs show either DRR or COR activity

The role of DRR in REPI as a gateway step into morphinan alkaloid biosynthesis together with a shared ancestry with COR, and their apparent ubiquity in the *Papaver* genus, suggest that DRR and COR are important components in the evolutionary history of the pathway. *DRR* and *COR* transcripts were categorized based on overall sequence identity compared with *P. somniferum DRR*(*REPI*) and *COR*, although a comparison of their catalytic tetrad motifs was a more robust feature to predict COR or DRR activity. COR-like transcripts possessed the canonical AKR tetrad, DYKH, whereas DRR-like transcripts contained the variations DYMP, DYML or DYNP. All enzymes containing the DYKH tetrad showed only COR activity, whereas all enzymes with either DYMP, DYML or DYNP motifs displayed only DRR activity. Six of the 12 CORs and 2 of the 11 DRRs showed weak activity detected only in long (overnight) assays (Figs. S5 and S6). Interestingly, the putative DRS-AKR fusion from *P. spicatum* contained the DYKH catalytic tetrad and showed weak COR activity, but not DRR activity (Fig. S6), suggesting a DRS-COR fusion. The REPI-like DRS-AKR transcript in *P. spicatum* contained the COR-like DYKH catalytic tetrad in its AKR moiety and exhibited COR activity (Fig. S6). Specific activities (Figs. 4 and 5) were measured for 9 DRRs and 6 CORs, and 4 representatives of each were further characterized (Tables 1, 2).

Unexpectedly, *P. somniferum* DRR(REPI) did not display the highest specific activity among DRR homologs in the *Papaver* genus. *P. bracteatum* DRR(REPI) displayed 2.7-fold higher reductive specific activity, whereas *P. radicatum*, *P. nudicaule* and *P. burseri* showed 7.2-, 6.2- and 5.6-fold higher reductive, and 10.1-, 4.8- and 5.0-fold higher oxidative activity, respectively, compared with *P. somniferum* DRR(REPI) (Fig. 4; Table S5). Kinetic characterization of *P. burseri* DRR showed a 1.3- and 6.2-fold increase in reductive and oxidative k_{cat}/K_m, respectively, compared with *P. somniferum* DRR(REPI) (Table 1, S5). *P. radicatum*, *P. nudicaule* and *P. burseri* DRRs are independent enzymes (i.e., not fused with DRS) that all share the DYML motif and are closely related in the *Meconella* section. The other tested DRRs belonging to the *Meconella* section, *P. miyabeanum* DRR1 and DRR2, contain the DYMP and DYNP motifs, respectively, showed 7.8- and 42.3-fold lower specific activity in the reductive assay, and 40.8- and 100.0-fold lower specific activity in the oxidative assay, respectively, compared with *P. somniferum* DRR(REPI) (Fig. 4; Table S5). Kinetic characterization of *P. burseri* DRR, *P. somniferum* DRR(REPI), *P. glaucum* DRR, and *P. lasiothrix* DRR(REPI) supported the observed trends in specific activity. Although less difference was apparent when comparing the reductive k_{cat}/K_m of *P. burseri* and *P. somniferum* DRR(REPI), and the oxidative k_{cat}/K_m of *P. lasiothrix* DRR(REPI) and *P. somniferum* DRR(REPI) (Table 1, S5)).

In contrast to the pattern of DRR activity, *P. somniferum* COR displayed the highest specific activity among COR homologs in the *Papaver* genus. Among the six enzymes that displayed the highest specific activity, *P. triniifolium* COR3 showed the most similar specific activity compared with *P. somniferum* COR (i.e., 3.6- and 1.2-fold lower with respect to reductive and oxidative reactions) (Fig. 5; Table S5). *P. triniifolium* COR2, *P. apokrinomenon* COR1, *P. glaucum* COR, and *P. apokrinomenon* COR2 showed 15.3-, 65.5-, 166.8-, and 917.5-fold lower specific activities in the reductive direction, whereas *P. triniifolium* COR2, *P. apokrinomenon* COR1 displayed 143.1- and 490.5-fold lower specific activity in the oxidative direction. k_{cat}/K_m for *P. somniferum* COR, *P. triniifolium* COR3, *P. apokrinomenon* COR1, and *P. glaucum* COR (Table 2, S5) supported trends in specific activity although *P. apokrinomenon* COR1 and *P. glaucum* COR showed a more dramatic decrease in reductive k_{cat}/K_m.

Among the *Papaver* AKRs, higher sequence identity to the *P. somniferum* enzyme (COR or DRR(REPI)) is correlated to increased activity among CORs but not DRRs (Table S6). The correlation suggests that *Papaver* CORs followed a more linear evolution compared with *Papaver* DRRs, which potentially followed a more branched evolutionary path. Unfused *Meconella* DRRs likely faced different selection pressures compared with fused DRR(REPI)s after divergence of the resulting lineages. The detection of highly active CORs in *P. triniifolium*, *P. apokrinomenon*, and *P. glaucum* was unexpected since none of these species accumulate COR substrates (i.e., codeinone or morphinone) or products (i.e., codeine or morphine). Moreover, only *P. triniifolium* accumulates even the pro-morphinan salutaridine (Fig. 1B).

AKR evolution and catalysis as revealed by *P. somniferum* DRR(REPI) mutagenesis

To investigate the atypical substitutions to the canonical AKR catalytic tetrad in DRRs, site-directed mutagenesis targeting the DYMP motif was applied to *P. somniferum* DRR(REPI) (Fig. 6). Two strategies were followed in mutant selection. First, substitutions were designed to negate the role of specific residues (E26A, E26D, E26Q, D51A, Y56A, Y56F, M86A, and

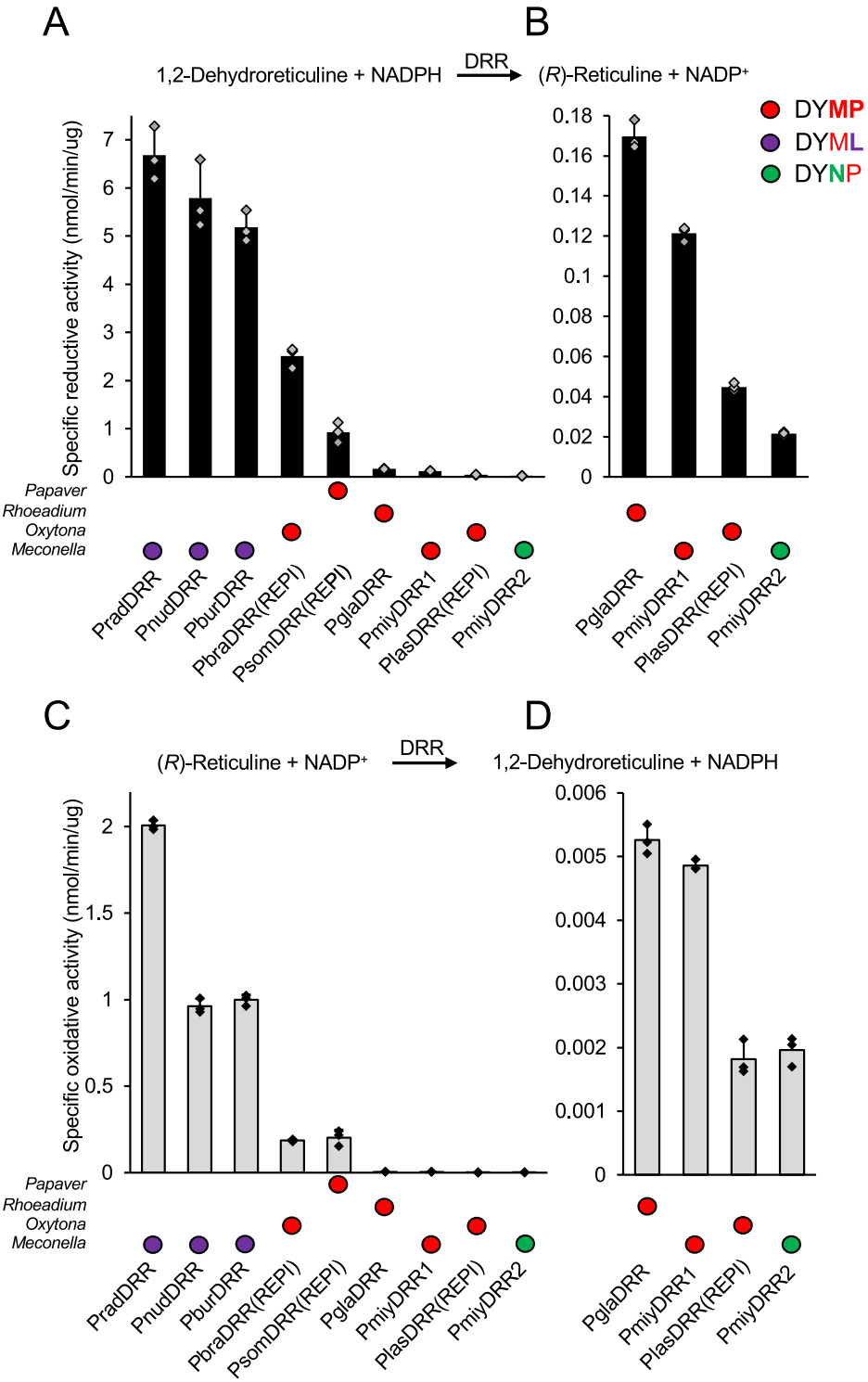

Fig. 4 | Functional characterization of DRR homologs from various *Papaver* species. Specific activities of select DRR homologs. Corresponding enzyme *Papaver* sections and catalytic tetrad motifs are shown underneath the X-axis and the reaction coordinate above the plots. **A**,**B** Black bars indicate specific activity in 'forward' reductive enzyme assays measuring the formation of (*R*)-reticuline from 20 μM 1,2-dehydroreticuline and 500 μM NADPH. Reactions were carried out in 100 mM Bis-tris propane buffer, pH 7.0. **A** Data for all characterized DRRs. **B** Data for a subset of DRRs with relatively low reductive activity. **C**,**D** Gray bars indicate specific activity in 'reverse' oxidative enzyme assays measuring the formation of 1,2-dehydroreticuline from 20 μM (*R*)-reticuline and 500 μM $NADP^+$. Reactions were carried out in 100 mM Bis-tris propane buffer, pH 8.8. **C** Data for all characterized DRRs. **D** Data for a subset of DRRs with relatively low oxidative activity. The protein concentrations and reaction times required to achieve less than 10% substrate conversion for each enzyme are provided in Table S10. Bars represent the mean ± standard deviation of three independent replicates.

P119A) and second, other substitutions were intended to reconstitute the canonical AKR catalytic tetrad of DYKH (M86K, P119H, and M86K-P119H). The E26 mutants were designed to investigate a hypothesized catalytic role of E26[29]. The mutants E26A, E26D, and E26Q showed 2.6-, 3.7-, and 19.5-fold decrease in reductive activity and 2.0-, 1.8-, and 3.5-fold decrease in oxidative activity, respectively (Fig. 6; Table S5). The retainment of modest to low DRR activity in the E26 mutants, particularly E26A, suggests that E26 plays a non-critical role in DRR catalysis. All mutations affecting the DYMP motif retained at least a low level of activity except for D51A in the oxidative direction, for which no activity was detected even in overnight assays. In the reductive direction, D51A showed a 4667-fold decrease in activity compared with wild type DRR(REPI), which represented the largest decrease in activity among the mutants (Fig. 6; Table S5). Y56A and Y56F substitutions showed the second largest decreases in activity (i.e., 1355- and 168-fold lower for the reductive reaction, and 7500- and 286-fold lower for the oxidative direction, respectively) compared with wild type DRR(REPI) (Fig. 6; Table S5). The higher activity of Y56F versus Y56A was expected, owing to the similarity of phenylalanine with tyrosine compared to alanine. It was nevertheless surprising that the Y56A and Y56F substitutions retain even a low level of activity based on the canonical importance of the titratable group contributed by Y56. Both D51 and Y56 are ubiquitously conserved across all AKR transcripts in the *Papaver* genus,

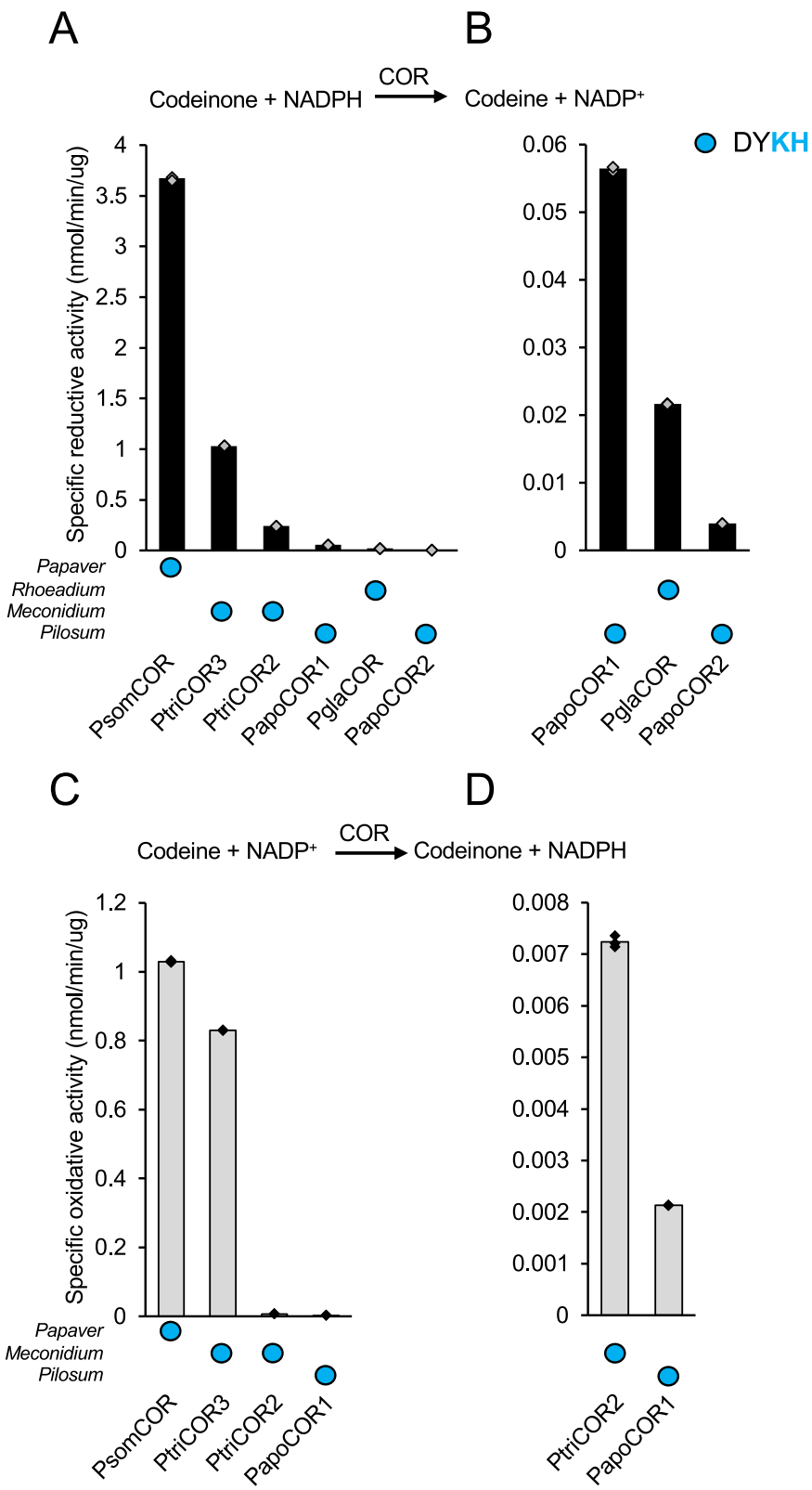

Fig. 5 | Functional characterization of COR homologs from various *Papaver* species. Specific activities of select COR homologs. Corresponding enzyme *Papaver* sections and catalytic tetrad motifs are shown underneath the X-axis and the reaction coordinate above the plots. **A**,**B** Black bars indicate specific activity in 'forward' reductive enzyme assays measuring the formation of codeinone from 50 μM codeine and 1 mM NADPH. Reactions were carried out in 100 mM Bis-tris propane buffer, pH 8.0. **A** Data for all characterized CORs. **B** Data for a subset of CORs with relatively low reductive activity. **C**,**D** Gray bars indicate specific activity in 'reverse' oxidative enzyme assays measuring the formation of 1,2-dehydroreticuline from 50 μM codeine and 1 mM $NADP^+$. Reactions were carried out in 100 mM Bis-tris propane buffer, pH 8.8. **C** Data for all characterized CORs. **D** Data for a subset of CORs with relatively low oxidative activity. The protein concentrations and reaction times required to achieve less than 10% substrate conversion for each enzyme are provided in Table S10. Bars represent the mean ± standard deviation of three independent replicates.

which coincides with substitutions resulting in the most detrimental effect on *P. somniferum* DRR(REPI) activity and highlighting their importance. M86 and P119 are less conserved across *Papaver* DRRs (i.e., natural M86N and P119L substitutions occur in active DRRs), although these positions are conserved as K86 and H119 across *Papaver* CORs. *P. somniferum* DRR(REPI) P119A and P119H substitutions resulted in a 60.0- and 6.5-fold decrease in activity for the reductive reaction, and a 105.9- and 9.5-fold decrease in the oxidative direction, respectively, compared with wild type DRR(REPI) (Fig. 6; Table S5). M86A and M86K substitutions resulted in 19.1- and 76.4-fold decreases in activity for the reductive reaction, and 6.2- and 8.6-fold decreases in the oxidative direction, respectively (Fig. 6; Table S5). The modest decrease in activity of M86 and P119 mutants and the observed natural amino acid substitutions at these positions among *Papaver* DRRs suggest that they are not required for catalysis. This is contrary to

Table 1 | Kinetic parameters of selected DRRs from various *Papaver* species

Enzyme	Substrate	Product	k_{cat} (s^{-1})	K_m (μM)	K_i (μM)	k_{cat}/K_m (M^{-1} s^{-1})
PburDRR	1,2-DR	(*R*)-R	5.40 ± 0.47	5.5 ± 1.0	79.5 ± 18.7	977,706
PsomDRR(REPI)	1,2-DR	(*R*)-R	5.36 ± 1.71	7.3 ± 2.2	43.9 ± 15.4	735,245
PglaDRR	1,2-DR	(*R*)-R	0.57 ± 0.05	16.4 ± 2.3	108.8 ± 23.4	35,078
PlasDRR(REPI)	1,2-DR	(*R*)-R	0.22 ± 0.02	12.3 ± 2.2	177.9 ± 63.2	17,544
PburDRR	(*R*)-R	1,2-DR	1.03 + 0.03	14.5 ± 1.8	NA	71,776
PsomDRR(REPI)	(*R*)-R	1,2-DR	0.43 + 0.01	37.3 ± 4.0	NA	11,559
PgalDRR	(*R*)-R	1,2-DR	0.31 + 0.04	906.6 ± 176.6	NA	340
PlasDRR(REPI)	(*R*)-R	1,2-DR	0.150 + 0.003	47.2 ± 2.9	NA	3097

Kinetic curves are shown in Fig. S17 and reaction conditions are provided in Table S12. K_i was determined from substrate inhibition curve fit. 'NA', not applicable, represents substrate inhibition was not observed. 1,2-dehydroreticuline is abbreviated as 1,2-DR and (*R*)-reticuline as (*R*)-R. Errors represent the mean ± standard deviation of three independent replicates.

Table 2 | Kinetic parameters of selected CORs from various *Papaver* species

Enzyme	Substrate	Product	k_{cat} (s^{-1})	K_m (μM)	k_{cat}/K_m (M^{-1} s^{-1})
PsomCOR	Codeinone	Codeine	3.33 ± 0.13	17.4 ± 1.6	191,331
PtriCOR3	Codeinone	Codeine	0.99 ± 0.03	10.0 ± 0.9	98,801
PapoCOR1	Codeinone	Codeine	0.0261 ± 0.002	116.8 ± 17.8	224
PglaCOR	Codeinone	Codeine	0.0236 ± 0.0007	78.8 ± 5.6	300
PsomCOR	Codeine	Codeinone	0.81 ± 0.03	49.9 ± 4.1	16,285
PtriCOR3	Codeine	Codeinone	0.39 ± 0.01	62.7 ± 5.2	6223
PapoCOR1	Codeine	Codeinone	0.0060 ± 0.0004	72.1 ± 9.4	89

Kinetic curves are shown in Fig. S18 and reaction conditions are provided in Table S12. Errors represent the mean ± standard deviation of three independent replicates.

CORs where K86 and H119, along with D51, form a proton relay promoting Y56 as general acid or base.

To investigate the apparent proton relay disruption, the canonical AKR catalytic tetrad of DYKH was reconstituted in *P. somniferum* DRR(REPI) by substituting M86K and P119H. The single substitutions retained a low level of DRR activity as described above, whereas the double substitution, M86K-P119H showed a 1063- and 327-fold decrease in DRR activity in the reductive and oxidative directions, respectively, compared with wild type DRR(REPI) (Fig. 6; Table S5). The M86K and M86K-P119H substitutions also exhibited a low level of COR activity (Fig. S7), which is attributed to the M86K substitution since no COR activity was detected with a P119H substitution. The low level of COR activity enabled by the M86K substitution is presumably caused by the reconstitution of a proton relay between D51, K86, and Y56.

Homology modeling and substrate docking of *Papaver* AKRs

The atypical DYMP motif in *P. somniferum* DRR(REPI) was further investigated by preparing a homology model of the holoenzyme bound to substrate and cofactor. Additionally, models of representative homologs possessing either the canonical AKR catalytic tetrad (DYKH) or one of the other observed substituted motifs (DYML or DYNP) were prepared. The DYKH catalytic tetrad was represented by the *P. somniferum* COR crystal structure (PDB: 7MBF), whereas homologs bearing the DYML and DYNP motifs were represented by homology models of *P. burseri* DRR and *P. miyabeanum* DRR2, respectively (Fig. 7, S8,S9). Homology models were prepared using *P. somniferum* COR crystal structure (PDB: 7MBF) as a template, and NADPH and alkaloid substrates were modeled by molecular docking.

The following structural analysis employs *P. somniferum* DRR(REPI) numbering unless stated otherwise. The modeled DRRs adopt the canonical AKR TIM-barrel fold from which the binding pocket is formed by five large loops (Fig. S8A), previously described[29]. The NADP(H) binding pocket is formed by loops B, C, β1α1, and β2α2 (Fig S8A). Inspection of the NADP(H) binding pocket reveal residues that are both positionally and sequentially conserved (G23, T24, E26, D51, Y56, N166, Q187, S214, L216, W223, A246, V261, V262, K263, S264, F265, E272, N273) while others are positionally conserved with substitutions (F/A/F/F25, A/A/A/G53, M/K/M/N86, P/H/L/P119, F/H/F/F120, S/C/S/S165, I/H/I/V213, S/A/S/S218, N/I/N/N219, G/C/G/G220, T/A/T/T221, L/M/M/M229, R/R/N/R269, L/S/L/L298) (Fig. S8B), *P. somniferum* DRR(REPI)/*P. somniferum* COR/*P. burseri* DRR/*P. miyabeanum* DRR2. *Papaver* AKR multiple sequence alignment shows further conservative substitutions to Q187, V261, and F265 (Fig. S10). Notably, the ring stacking interaction between residue 213 and the nicotinamide ring of NADP(H) is not conserved in REPI/DRRs, where the typically aromatic 213 is substituted with a short aliphatic residue (Fig. 7, S8B)), even though this distinctive structural feature is highly conserved with the AKR superfamily[40]. Other residues and key interactions between protein side chains and NADP(H) are well conserved, as observed across the entire AKR superfamily: carboxamide side chain (S/C165, N166, Q190), nicotinamide ribose (D51, T24), pyrophosphate backbone (L216, S214), and adenosine 2'-monophosphate (S264, F265, R269*, E272, N273)[40]. R269 is substituted with an asparagine in several DRRs, but the carboxamide side chain likely still mediates hydrogen-bond interactions with the adenosine 2'-monophosphate of NADP(H) that are functionally similar with the guanidino functional group of arginine (Fig. S8B).

The substrate binding pocket is formed by contributions from all five loops (Fig. S8A). Closer inspection reveals the conservation of key residues (E26, Y56, W88, I133, W223, F302) and substitutions to residues (V/M/E/V28, A/A/A/S55, C/C/F/C89, P/H/L/P119, F/H/F/F120, M/N/M/M131, L/S/L/L298, S/S/D/T299, Y/N/H/N301), *P. somniferum* DRR(REPI)/*P. somniferum* COR/*P. burseri* DRR/*P. miyabeanum* DRR2 (Fig. 7). *Papaver* AKR multiple sequence alignments show additional substitutions to I133, L198, and minimally F302 (Fig. S10). Exclusive to the *Meconella* DYML DRRs is the conservation of E28, F89, and H301. F89 is otherwise substituted by cysteine, serine, or glycine in other homologs, whereas E28 is substituted with methionine in *P. somniferum* COR and its two most similar homologs, and otherwise primarily substituted by a short aliphatic residue. Position 301 is primarily conserved as an aspartic or glutamic acid in CORs and weak

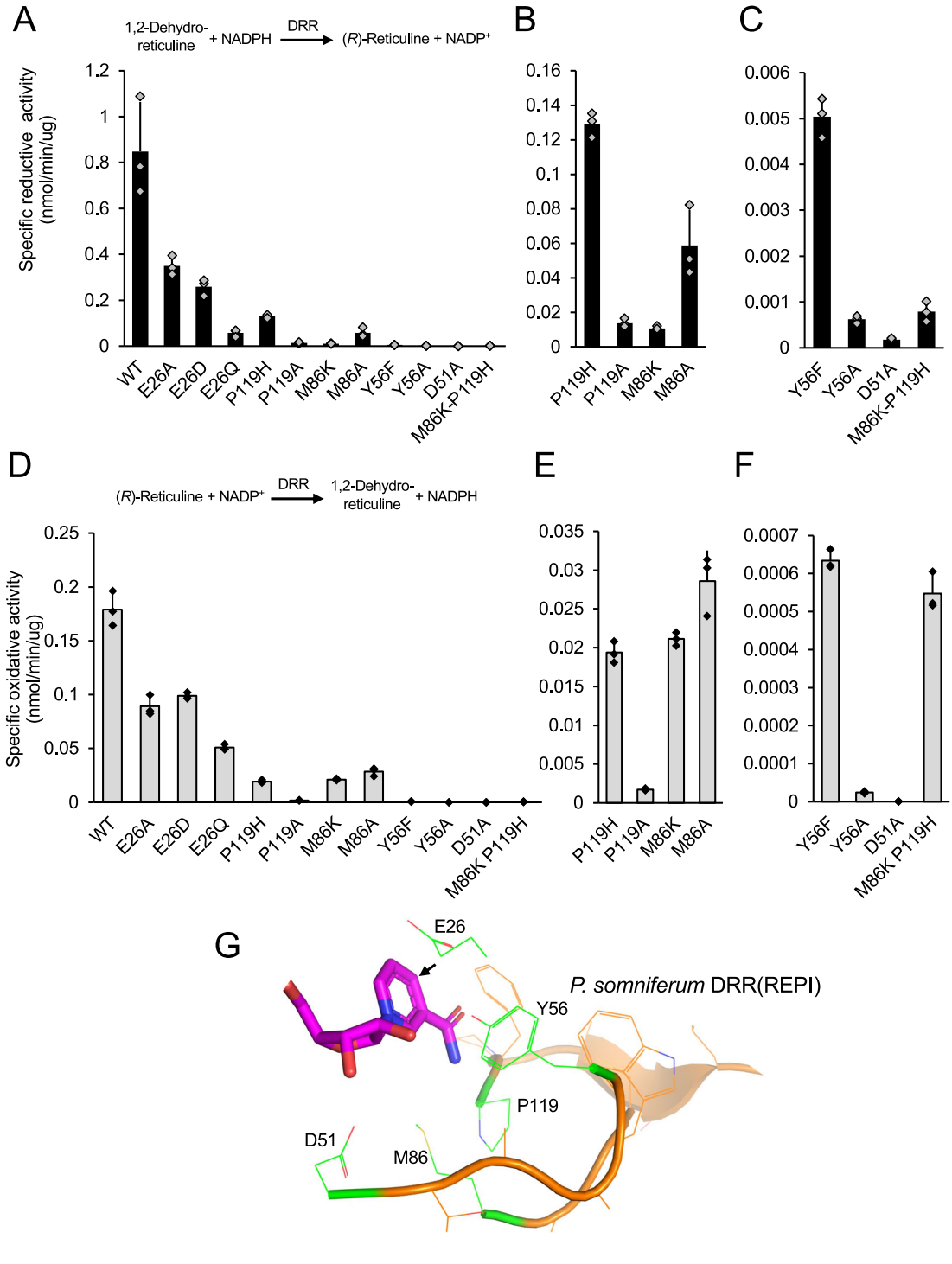

Fig. 6 | Mutagenesis of the DRR component of REPI from opium poppy reveals a novel catalytic tetrad. A–C Black bars indicate specific activity of DRR mutants in 'forward' reductive enzyme assays measuring the formation of (*R*)-reticuline from 20 μM 1,2-dehydroreticuline and 500 μM NADPH. Reactions were carried out in 100 mM Bis-tris propane buffer, pH 7.0. **A** Data for all characterized DRRs. **B** Data for a subset of DRRs with relatively moderate reductive activity. **C** Data for a subset of DRRs with relatively low reductive activity. **D–F** Gray bars indicate specific activity of DRR mutants in 'reverse' oxidative enzyme assays measuring the formation of 1,2-dehydroreticuline from 20 μM (*R*)-reticuline and 500 μM $NADP^+$. Reactions were carried out in 100 mM Bis-tris propane buffer, pH 8.8. **D** Data for all characterized DRRs. **E** Data for a subset of DRRs with relatively moderate oxidative activity. **F** Data for a subset of DRRs with relatively low oxidative activity. The protein concentrations and reaction times required to achieve less than 10% substrate conversion for each enzyme are provided in Table S11. Bars represent the mean ± standard deviation of three independent replicates. Reaction coordinates are shown above the plots. **G** Depiction of the active site residues selected for mutagenesis from the homology model of *P. somniferum* DRR from REPI. Mutagenesis candidate residues are shown in green, NADPH in magenta, and the pro R face of NADPH is designated with an arrow.

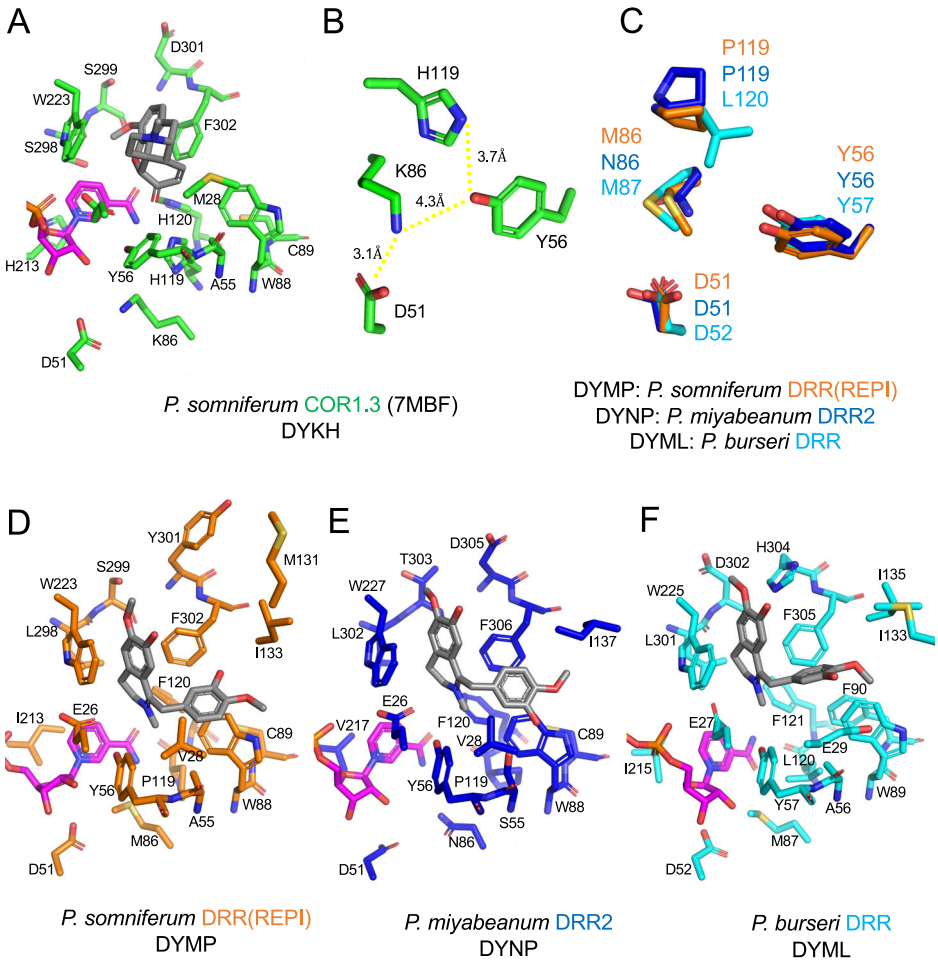

Fig. 7 | Characterization of the binding pocket in AKRs from various Papaver species. A Crystal structure of COR (7MBF) from opium poppy (*P. somniferum*)[29] shown in green. **B** Arrangement of the catalytic tetrad in COR from *P. somniferum*. **C** Superposition of the respective motifs of substitutions to the canonical AKR catalytic tetrad in *P. somniferum* DRR(REPI) (orange), *P. miyabeanum* DRR2 (blue), and *P. burseri* DRR (cyan). **D** the DRR component of REPI from *P. somniferum* shown in orange, (**E**) DRR2 from *P. miyabeanum* shown in blue, and **F** DRR from *P. burseri* shown in cyan. In all cases, a docked molecule of NADPH is shown in magenta and docked ligand molecules (i.e., codeinone for COR and 1,2-dehydroreticuline for DRR) are shown in gray. Carbon atoms are represented by the base color of each enzyme, with red corresponding to oxygen, blue to nitrogen, and yellow to sulfur. Hydrogen bonding and electrostatic interactions are shown in yellow (predicted) and red (disrupted) dashed lines. Red arrows depict predicted movements of sidechains and substrates based on binding pocket residue substitutions. PyMOL was used to generate images of the models[82].

REPI/DRRs (*P. glaucum* DRR being to most active of these (Fig. 4)) and is a tyrosine in REPI homologs (excluding the weak *P. lasiothrix* REPI). Position 131 is more generally conserved as a methionine in REPI/DRRs and displays more variability in CORs. Coordination between all four catalytic residues is evident in the COR catalytic tetrad (DYKH) (Fig. 7B)[29], where H119, K86, and D51 act to alter the apparent pK_a of Y56[23]. Substitutions to the canonical AKR catalytic tetrad observed in DRRs (i.e., DYMP, DYML, and DYNP) preclude the formation of the canonical hydrogen-bonding network with Y56 (Fig. 7C). This, alongside the loss of H213 stacking with the nicotinamide ring of NADP(H) and mutagenesis results, suggests that some homologs may utilize an alternative catalytic mechanism lacking some of the features assisting with the general acid/base functions of Y56 and allowing for slightly altered orientations of NADP(H). Additionally, E26[29] and K27[41] have been proposed as alternative catalytic residues to act in place of the substituted lysine and histidine in *P. somniferum* DRR(REPI). Retention of modest to low DRR activity in the site-directed mutants generated for E26 suggests roles for the side chain of this residue in substrate binding or coordination, but the side chain does not appear to play a critical role in catalysis (Fig. 6). K27 was not included in our mutagenesis and is conserved in REPIs and several CORs, but it is commonly substituted with threonine in DRRs (Fig. S10). The lack of K27 conservation between REPI and DRRs raises questions about its proposed roles in catalysis. However, both substitutions possess titratable sidechains and thus cannot be discredited without proper biochemical analysis.

This work is complementary to our previous modeling of *P. somniferum* DRR(REPI)[29] and more recent AlphaFold modeling and molecular dynamics analyzes of *P. somniferum* REPI[41]. Investigation of the DRR(REPI) model generated by molecular dynamics (as shown in Fig. 6 from[41]) alongside a superposition of the AlphaFold REPI model (https://alphafold.ebi.ac.uk) with our DRR(REPI) homology model reveal several similarities and differences. All three models suggest that substitutions to the canonical AKR catalytic tetrad residues (K86 and H119) are unlikely to alter the architecture of the active site, but the loss of functional groups created by these substitutions suggest a more simple catalytic mechanism or that alternate functional groups for catalysis may be supplied by the side chains at nearby positions: E26[29] and K27[41]. The molecular dynamics study[41] proposed an alternate mode of 1,2-dehydroreticline binding characterized by a more closed conformation of loop A, pushing 1,2-dehydroreticuline deeper into the TIM-barrel (Fig. S9). In the absence of experimentally determined REPI or DRR structures, the validity of these models should be cautiously assessed.

Functional characterization of *Papaver* DRS, DRR, REPI and SalSyn in yeast

To further investigate the gateway into morphinan alkaloid biosynthesis across the *Papaver* genus, available *DRS*, *DRR*, *REPI*, and *SalSyn* orthologs were characterized in engineered yeast. The anchor domains of *Papaver* CYPs were modified to promote membrane insertion empirically more conducive to catalytic activity[42,43] (Table S7). Engineered *DRS* orthologs from *P. rhoeas*, *P. triniifolium*, *P. nudicaule*, and *P. burseri* transiently expressed in yeast with genome-integrated benzylisoquinoline uptake permease 1 (*BUP1*) and cytochrome P450 reductase 2 (*CPR2*) were able to convert (*S*)-reticuline to 1,2-dehydroreticuline (Figs. 8A and S11). Congruent to in vitro characterization, DRR orthologs from *P. nudicaule*, *P. burseri*, and *P. spicatum* converted 1,2-dehydroreticuline to (*R*)-reticuline when transiently expressed in yeast with genome-integrated BUP1 and CRP2 (Figs. 8D and S12). *Papaver REPI* orthologs from *P. somniferum, P. lasiothrix*, and the putative DRS-COR fusion from *P. spicatum* were

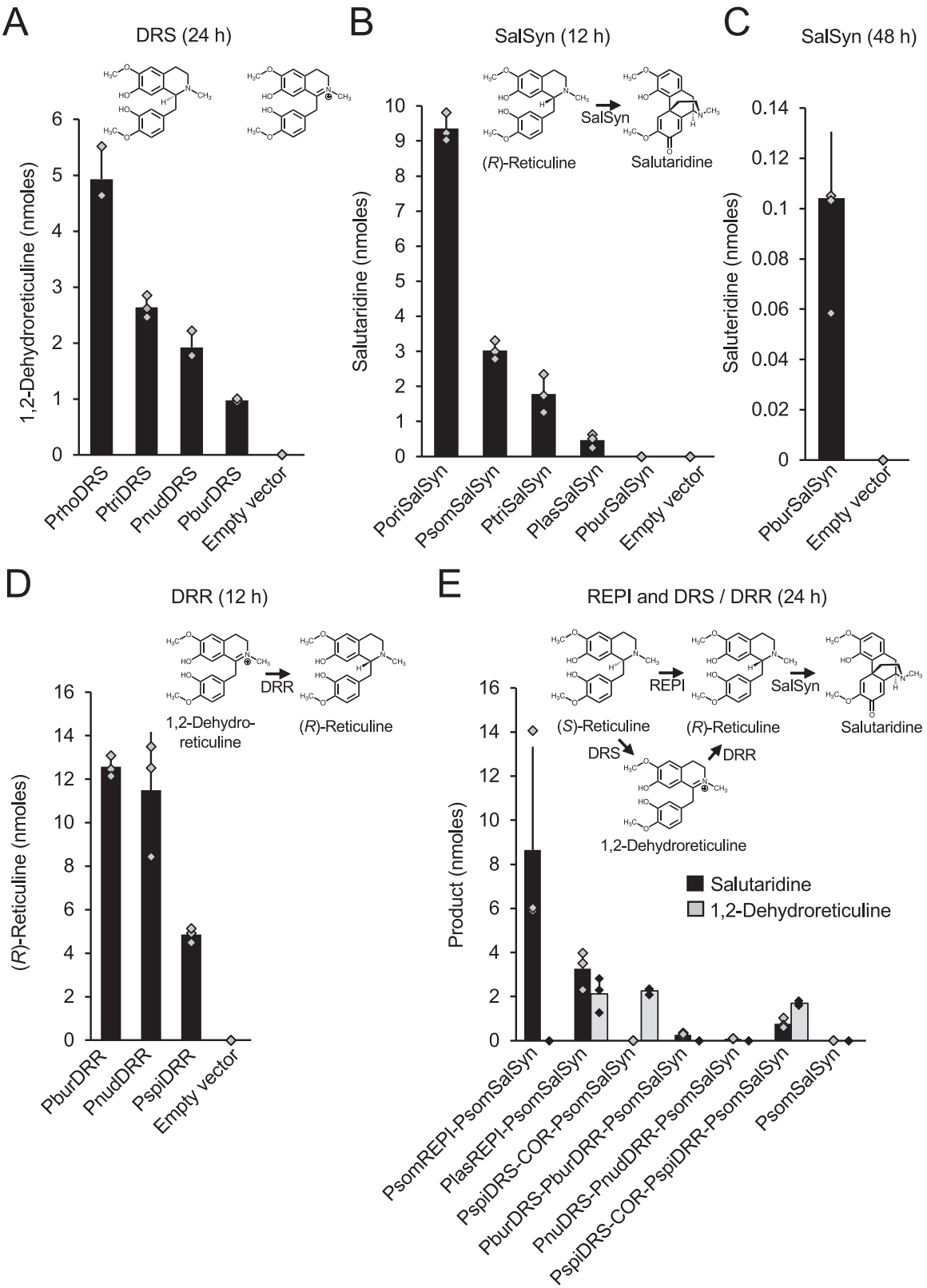

Fig. 8 | Functional characterization of DRR, DRS, REPI, and SalSyn homologs from various Papaver species in engineered yeast strains. A DRS, (**B**,**C**) SalSyn, (**D**) DRR, (**E**) REPI and unfused DRS-DRR pairs were transiently expressed in one of two yeast strains: (i) a BUP1- and CPR2-chromosomally integrated strain (used for DRS, SalSyn and DRR) and (ii) a BUP1-, CPR2- and SalSyn-chromosomally integrated strain (used for REPI, and unfused DRS and DRR pairs). Yeast strains were feed 50 µM of the indicated substrate (i.e., (*S*)-reticuline for DRS, (*R*)-reticuline for SalSyn, 1,2-dehydroreticuline for DRR, and (*S*)-reticuline for REPI, and unfused DRS and DRR pairs. Yeast cultures were incubated for the indicated time (i.e., 12, 24 or 48 h) and conversion products (i.e., 1,2-dehydroreticuline for DRS, salutaridine for SalSyn, (*R*)-reticuline for DRR, and salutaridine, (*S*)-reticuline and 1,2-dehydroreticuline for REPI, and unfused DRS and DRR pairs) were detected and quantified using a five-point standard curve. Error bars correspond to the mean ± standard deviation of three biological replicates (i.e., three independent colonies). The catalyzed reaction and sequences are shown above each plot.

transiently expressed in yeast with genome-integrated *P. somniferum SalSyn*, *BUP1*, and *CPR2*, in which the (*R*)-reticuline produced from (*S*)-reticuline by REPI was further converted to salutaridine by SalSyn, allowing detection of REPI activity without chiral separation of (*S*/*R*)-reticuline. *P. somniferum* and *P. lasiothrix REPI* orthologs converted (*S*)-reticuline as shown by the detection of salutaridine (Figs. 8E and S13A). Unlike yeast expressing *P. somniferum REPI*, in which only salutaridine was detected, yeast expressing *P. lasiothrix REPI* also accumulated 1,2-dehydroreticuline suggesting that the DRR domain is less efficient than the DRS component of the fusion protein (Figs. 8E and S13A). This result is consistent with the kinetic characterization of *P. lasiothrix* DRR(REPI), which showed a 39-fold decrease in catalytic efficiency compared with *P. somniferum* DRR(REPI) (Table 1). The putative *P. spicatum* DRS-COR fusion showed DRS activity by converting (*S*)-reticuline to 1,2-dehydroreticuline, although (*R*)-reticuline was not detected. This result is also consistent with the in vitro characterization of *P. spicatum* COR(DRS-COR), which showed COR, but not DRR, activity (Fig. S6). The COR activity associated with the *P. spicatum* DRS-COR fusion was also confirmed in transformed yeast (Fig. S13B). However, transient expression of the *P. spicatum* DRS-COR fusion, together with unfused *P. spicatum DRR* in yeast containing integrated *SalSyn*, *BUP1*, and *CPR2* resulted in the conversion of (*S*)-reticuline to (*R*)-reticuline, evident by the accumulation of salutaridine (Figs. 8E and S14A). In this case, (*S*)-reticuline was apparently converted to 1,2-dehydroreticuline by *P. spicatum* DRS(DRS-COR) and subsequently converted to (*R*)-reticuline by the unfused *P. spicatum* DRR. Similarly, unfused *DRS* and *DRR* orthologous pairs from *P. burseri* and *P. nudicaule* also converted (*S*)-reticuline to (*R*)-reticuline, which was shown by the detection of salutaridine (Figs. 8E and S14A), suggesting that unfused DRS and DRR enzymes can catalyze the conversion of (*S*)-reticuline to (*R*)-reticuline in these species. The DRS-COR fusion converted (*S*)-reticuline to (*R*)-reticuline when expressed in yeast (Figs. 8E and S13A).

Finally, *P. orientale, P. somniferum, P. triniifolium, P. lasiothrix*, and *P. burseri SalSyn* orthologs were transiently expressed in yeast with genome integrated *BUP1* and *CPR2*, and all showed SalSyn activity, evident by the conversion of (*R*)-reticuline to salutaridine (Figs. 8B,C and S15). None of the enzymes encoded by these *SalSyn* orthologs accepted (*S*)-reticuline. Importantly, identity of the *SalSyn* ortholog from *P. burseri* was confirmed.

Discussion

Herein, we demonstrate the widespread occurrence across the genus *Papaver* of orthologous genes putatively encoding morphine biosynthetic enzymes, notably in several species that do not accumulate pro-morphinan or morphinan alkaloids. In vitro characterization of enzymes encoded by *DRR* and *COR* orthologs revealed the latency and ubiquity of DRR and COR activities in the genus *Papaver* and, more unexpectedly, the occurrence of enzymes with specific activities higher than those found in *P. somniferum*. Whereas highly active DRRs could potentially participate in the stereochemical inversion of (*S*)-reticuline in salutaridine biosynthesis, highly active CORs in species that do not accumulate morphinan alkaloids (i.e., *P. triniifolium P. glaucum*, and *P. apokrinomenon*) cannot be explained according to the canonical function of COR. Although not functionally characterized in this study, similar trends are apparent for the ubiquitous *CODM* and *NISO* orthologs, and the more taxonomically restricted *SalR*, *SalAT*, and *THS* orthologs. We present two hypotheses to explain these phenomena, which could at least partially explain the presence of morphinan alkaloid biosynthetic enzymes in *Papaver* species that do not accumulate pro-morphinan or morphinan alkaloids.

In one hypothesis, *DRR* and *COR* genes in the genus *Papaver* could be remnants of ancestral pro-morphinan or morphinan biosynthetic pathways that have been partially lost, leaving behind a latent biosynthetic fingerprint. This has been proposed in the broader context of BIA biosynthesis in angiosperms not known to accumulate BIAs based on phylogenetic analysis of norcoclaurine synthase (NCS), berberine bridge enzyme, and selected *O*-methyltransferases[44]. Recently, characterization of REPI from the non-morphinan producing *P. californicum* was also suggested to be a remnant of ancestral pro-morphinan alkaloid biosynthesis[15]. Assuming monophyletic origin, the lack of pro-morphinan biosynthetic enzymes in species that diverged after the earliest known occurrence of pro-morphinan biosynthesis can be attributed to gene deletion[15].

In a second hypothesis, several morphinan alkaloid biosynthetic enzymes could be multifunctional with roles in other metabolic pathways. This is especially attractive for the DIOX enzymes, which display broad BIA substrate ranges[36]. CODM was shown to be potentially involved in the biosynthesis of protopines and protoberberines, in addition to its role in morphinan alkaloid biosynthesis. Based on the purported emergence of protopine and protoberberine alkaloid biosynthesis before the divergence of the *Papaver* genus[44], the ubiquitous distribution of CODM-like transcript in *Papaver* species could be the result of orthologous roles in other BIA biosynthetic pathways. CORs in the *Papaver* genus might also be multifunctional, although substrates other than morphinan alkaloids have not been tested. Latent CORs may represent ancestral AKRs, with separate physiological roles, later recruited into morphinan alkaloid biosynthesis based on their non-canonical ability to convert codeinone to codeine. Similar reasoning can be applied to other morphinan biosynthetic enzymes including SalR, which is involved in the conversion of salutaridine to thebaine, having also been shown to occur widely in the genus *Papaver* beyond a correlation with thebaine distribution[45]. This hypothesis, however, does not explain the occurrence, in non-morphinan producing *Papaver* species, of high amino acid sequence identity and highly active COR enzymes. These features are most likely remnants of an ancient morphinan alkaloid biosynthetic pathway.

These hypotheses align with the patchwork model of pathway evolution, which has been recently suggested for morphinan alkaloid biosynthesis[14], whereby a limited number of key evolutionary events bridge gaps between clusters of pre-existing latent biosynthetic enzymes. The background of latent enzymes, dubbed 'underground metabolism', provides a foundation for the emergence of novel biosynthetic pathways[22]. Gene duplication, either through whole genome or local replication processes, provides new genetic material for the recruitment of novel enzymes without disrupting existing biological functions. The focus of this work was the emergence of the AKRs DRR and COR, however intriguing patterns in transcript distribution particularly in the DIOX family merit discussion. Additionally, the taxonomical restriction of SalSyn- and T6ODM-like transcripts to salutaridine and thebaine-producing *Papaver* species suggests their emergence be important evolutionary events. SalSyn catalyzes the formation of the pro-morphinan scaffold, which represents a potentially selective trait. Recruitment of T6ODM, possibly from its closest and potentially more widespread paralog PODA, which exhibits latent T6ODM activity[36], could facilitate the formation of codeine and morphine. In pyrrilizidine alkaloid biosynthesis, homospermidine synthase was recruited from the primary metabolic enzyme deoxyhypusine synthase, which demonstrates latent homospermidine synthase activity[46]. Additionally, caffeine biosynthesis arose several times independently from benzoate and salicylate *O*-methyltransferases harboring latent xanthine *N*-methyltransferase activity, which has been maintained for over 100 million years[19]. Moreover, recent work on the characterization of PR10 proteins from *P. somniferum* suggests that the enzymes NCS, THS and NISO evolved from BIA binding proteins[47]. Binding affinity may be considered a form of pre-enzymatic latency, from which neofunctionalization can yield novel enzyme function[48,49].

A growing body of research has highlighted the importance of transcriptional regulation in the evolution of specialized metabolism[50], including BIA biosynthesis[14,51,52]. The evolution of regulatory elements, such as transcription factors, has been proposed in plant specialized metabolism, specifically nicotine biosynthesis in the genus *Nicotiana*[53,54]. Whole genome triplication in the *Solanaceae* family is thought to have led to an enrichment of transposable elements responsible for the derivation of new transcription factor binding sites and subsequent root-specific expression of nicotine biosynthetic genes[54]. In this case, whole genome triplication not only contributes to the neofunctionalization of duplicated primary metabolic genes,

but also provides a mechanism for the evolution of gene regulation. Based on the localized expression of pro-morphinan and morphinan alkaloid biosynthetic enzymes in either sieve elements and/or laticifers of *P. somniferum*, similar processes could be relevant in BIA metabolism.

Given that DRR and COR are the only AKRs known to be involved in BIA biosynthesis, the inferred evolutionary history of these two enzymes help to shed light on how genes and enzyme activities can be recruited and modified to catalyze distinct steps during the evolution of complex metabolic pathways. The AKR superfamily is a diverse family of enzymes found in all phyla, possessing a well conserved canonical catalytic tetrad DYKH and most commonly catalyzing the relatively simple reduction of carbonyl oxygens[23]. However, variations in catalytic tetrads and chemical reactivity have also been observed[23,27,28]. We show that CORs possess the canonical AKR catalytic tetrad of DYKH, whereas DRRs possess atypical DYMP (as previously documented in *P. somniferum* DRR(REPI)[29]) and the newly documented DYML or DYNP tetrads. The K86M/N and H119P/L substitutions in DRR motifs clearly disrupt their canonical role in altering the apparent pK_a of Y56, as demonstrated in structural analysis and supported by activity assays of mutants at positions 86 and 119 in *P. somniferum* DRR(REPI). Congruently, reconstitution of the D-K-Y proton relay in *P. somniferum* DRR(REPI) by the gain-of-function M86K mutant allowed for the reduction of codeinone and oxidation of codeine. Parallel to the catalytic tetrad substitutions, DRRs possess the atypical loss of aromaticity at position 213 which canonically interacts with the nicotinamide ring of NADP(H), from which the hydride is donated or accepted. These patterns suggest that the catalysis of reduction of 1,2-dehydroreticuline does not strictly require alterations of pK_a in Y56 by K86 and H119, and perhaps is more tolerant of suboptimal orientations of the hydride donor and the substrate. This is supported by the higher reactivity of 1,2-iminium ion substrates[55]. Similar alterations to canonical catalytic residues have also been observed in alcohol dehydrogenases (ADHs) with biosynthetic roles in monoterpene indole alkaloid (MIA) biosynthesis catalyzing 1,4- and/or 1,2-iminium ion reductions[56–59]. Substitutions to typically conserved residues involved in both proton relay and zinc ion coordination have led to the suggestion that the proper positioning of the reactive iminium ion substrate and NADPH is sufficient for reduction to occur in the absence of general acid/base catalysis[56]. DRR, and MIA ADHs are structurally different than other imine reductases (IREDs) which typically possess the conserved IRED fold[60,61]. IRED imine reductions typically proceed through enzyme catalyzed protonation of the imine substrate to form an iminium ion intermediate, which is readily reduced by NADPH[60,62–64]. 1,2-Dehydroreticuline, like most substrates of the atypical MIA ADHs, is present as an iminium ion; thus, the initial imine protonation observed in IREDs is not required. DRR and the atypical MIA ADHs demonstrate an intriguing case of convergent evolution, in which iminium ion reduction was recruited in independent alkaloid biosynthetic pathways, BIA and MIA, from different classes of reductive enzymes, AKRs and ADHs, respectively. As proposed for atypical MIA ADHs, reduction of the iminium ion form of 1,2-dehyroreticuline by DRR might only require proper coordination of the substrate and cofactor allowing for hydride attack at the C1 carbon to yield (*R*)-reticuline. Alternative catalytic residues, E26[29] and K27[41], have been proposed for *P. somniferum* DRR(REPI). Our mutagenesis studies of *P. somniferum* DRR(REPI) do not support the catalytic involvement of E26, while lack of conservation within DRRs questions the contribution of K27. Additionally, the apparent reactivity of 1,2-dehydroreticuline requiring only hydride attack without protonation/deprotonation, suggests that the catalytic mechanism of DRR may not require additional titratable residues to assist with the hydride transfer reaction. 1,2-Dehydroreticuline has been shown to exist as an iminium ion and in basic conditions, an enamine[65]. However, feeding experiments in *P. somniferum* suggest that iminium ion to enamine conversion does not occur[66]. As illustrated by molecular dynamics simulations of REPI[41], the fusion of DRS and DRR in REPI is expected to promote the channeling of the 1,2-dehydroreticuline produced by DRS to DRR, precluding enamine formation. However, substrate channeling between separate DRS and DRR enzyme molecules has not been demonstrated, and it is more likely that 1,2-dehydroreticuline occurred in its enamine form in earlier *Papaver* species, prior to the REPI fusion. This provides an ancestral role for Y56 and other accessory catalytic residues, in which general acid/base catalysis could assist with the conversion of the enamine to the 1,2-dehydroretciuline iminium ion to assist with its reduction to (*R*)-reticuline. This scenario also suggests that metabolic channeling may have provided more selective pressure for the REPI fusion event than catalytic enhancement.

Interestingly, a single M86K substitution in the *P. somniferum* DYMP catalytic tetrad, which partially reconstituted the canonical DYKH tetrad, resulted in a bifunctional DRR/COR enzyme. Structural analysis by homology modeling and molecular docking suggests that the partial reconstitution of the canonical DYKH tetrad as DYKP allows K86 and D51 to promote Y56 protonation/deprotonation of the substrate. This demonstrates that a single amino acid substitution is sufficient to toggle latent enzymatic activity, yielding a different enzyme with the potential to participate in specialized metabolism. The recruitment of xanthine methyltransferase occurred repeatedly during the convergent evolution of caffeine biosynthesis from latent enzyme activity facilitated by single proline to serine and histidine to asparagine substitutions in an ancestral methyltransferase[19]. Other examples of perturbations to enzyme specificity are reviewed in ref. 67, including cases in glucosinolate biosynthesis[68] and acyl-sugar biosynthesis[69]. These examples demonstrate the relative ease with which latent activities can be neofunctionalized and, subsequently, undergo selection.

Owing to its broad conservation across plant AKRs[70] and placement in the same orthogroup, DRR and COR likely evolved from a common AKR ancestor. Presumably, the DRR/COR AKR ancestor possessed the canonical DYKH catalytic tetrad, and single or double amino acid substitutions forming the DYMP motif led to neofunctionalization and subsequent selection of DRR. The DYMP motif is most widespread, being associated with *P. somniferum* DRR(REPI) and DRRs in the more distantly related *Meconella* section and, thus, assumed to be the ancestral DRR catalytic tetrad. Interestingly, the DYML DRR motif, and several other substrate binding pocket residues are only conserved in the *Meconella* section, in *P. radicatum, P. burseri*, and *P. nudicaule*, corresponding to DRRs with higher activity compared with *P. somniferum* DRR(REPI). *P. burseri*, and *P. nudicaule* were also shown to accumulate salutaridine, suggesting that their DRRs are involved in the stereochemical inversion of (*S*)-reticuline. Neofunctionalization leading to COR is less straightforward in the absence of a clear structural marker such as the DRR motifs. COR catalyzes the canonical reduction of a carbonyl oxygen and might have emerged from the general promiscuity of the AKR family. Our study failed to identify native *Papaver* AKRs lacking both COR and DRR activity. Ancestral enzyme reconstruction or analysis of AKRs beyond the *Papaver* genus could better define the structural underpinnings of COR evolution.

The *Meconella* species, *P. burseri* and *P. nudicaule*, both accumulate salutaridine and possess transcripts for unfused DRS and DRR orthologs in place of REPI, consistent with the recently published draft genome of *P. nudicaule*[15]. The conversion of (*S*)-reticuline to (*R*)-reticuline in these species is apparently catalyzed by unfused DRS and DRR enzymes. Importantly, these findings suggest that the stereochemical inversion of (*S*)-reticuline emerged prior to the REPI fusion from previously functionalized *DRS* and *DRR* orthologs and before the divergence of the *Meconella* section. Following this hypothesis, the fusion event yielding REPI likely occurred after the *Meconella* divergence and before the emergence of *P. californicum*, potentially under the selective pressure of enhancing pro-morphinan alkaloid accumulation, rather than being the pivotal step in its evolution as previously suggested[14–16]. In addition to precluding enamine formation and taking into consideration the prevalence of gene clusters in BIA metabolism[71], the REPI fusion can be considered the ultimate in 'gene clustering', ensuring spatial/temporal co-expression of *DRS* and *DRR* as a means of optimizing the formation of (*R*)-reticuline and downstream pathway intermediates. A summary of the proposed, revised evolutionary history of pro-morphinan and morphinan biosynthesis in the genus *Papaver* is illustrated in Fig. S19.

Mapping the pro-morphinan and morphinan alkaloid genetic landscape in the genus *Papaver* is revealing a dynamic evolutionary history involving the existence of promiscuous catalysts with latent functions, multifunctional enzymes, remnants of ancestral biosynthetic pathways, and only marginally understood transcriptional regulation. Our work contributes to the narrative that evolution of the intriguing REPI fusion protein represents a significant step in the process[15,16]. Our systematic and mechanistic analyzes of AKRs from the *Papaver* genus highlight the timing and structural features relevant to the evolution of pro-morphinan and morphinan alkaloids, serve as a model to understand the evolution of plant specialized metabolism in general.

Methods

Chemicals

Codeinone, 1,2-dehydroreticuline, and salutaridine were purchased from Toronto Research Chemicals (https://trc-canada.com/). (*S*)-Reticuline and (*R*)-reticuline were purchased from Cayman Chemicals (https://caymanchem.com/). Codeine was a gift from Sanofi-Aventis (https://www.sanofi.com/).

Plant material

Papaver seeds were obtained from Plant World Seeds (https://plant-world-seeds.com) and were cultivated in growth chambers at 20/18 °C (light/dark) with a 16-h photoperiod with cool white fluorescent and incandescent lights. Rosette stems with leaves removed at their base were harvested from three independent plants grown to anthesis. Rosette stems were flash frozen using liquid nitrogen and stored at −80 °C until used for RNA and or alkaloid extraction. Tissues were extracted with 1.2 mL acetonitrile and centrifuged (10,000 *g*) to remove insoluble debris, which was extracted twice with 500 µL acetonitrile, centrifuged after each extraction, and all supernatants were combined in a fresh tube. The remaining insoluble debris was used to determine the dry weight of each sample for normalization purposes. The insoluble debris was heated to 60 °C under vacuum for 3 days for complete desiccation prior to weighing. To ensure a narrow dynamic range of metabolites in the high-resolution liquid chromatography-mass spectrometry (LC-MS) analysis, dry weights were also used to adjust supernatant concentrations between replicates so that all extracts corresponded to an equivalent amount of dry matter. Following this adjustment, 500 µL from each acetonitrile extract was diluted 1:100 or 1:1000 with acetonitrile. *P. somniferum* was grown with appropriate license and government approval.

Transcriptomes

RNA from *Papaver* species was extracted using the trimethyl ammonium bromide (CTAB) method[72] from frozen rosette stems, which were ground to a fine powder using a TissueLyser (Qiagen; Hilden, Germany). Libraries were prepared using the NEBNext Ultra II Directional RNA Library Prep Kit (New England Biolabs). Illumina sequencing and transcriptome assembly were performed at the Genome Quebec Innovation Center (http://gqinnovationcenter.com/index.aspx/) based on HiSeq PE100 (Illumina; San Diego, CA) (Table S8). Previously published transcriptomes were included in our analyzes. Short read assemblies (SRAs) were assembled using trinity for *Roemeria refracta* (SRR19536717)[34]. NCBI transcriptome shotgun assemblies were used for *P. dubium* (GJOS00000000), *P. bracteatum* (GJOQ00000000), *P. orientale* (GJOT00000000), *P. armeniacum* (GJOO00000000), *P. californicum* (GJOY00000000), and *P. pavonium* (GJOU00000000)[15]; and *Argemone mexicana* (GJVJ00000000)[33]. The One Thousand Plant Transcriptomes database was used for *P. rhoeas*[31,32]. Transcripts were annotated based on sequence identity to *P. somniferum* morphinan biosynthetic enzymes, with a 60% sequence identity cut-off (Table S2). Transcripts were omitted if higher sequence identity to a different biosynthetic enzyme was observed. For example, many SalSyn-like transcripts above 70% identity to somniferum SalSyn showed over 90% identity to cheilanthifoline or stylopine synthase. In these obvious cases, transcripts were not assigned 'SalSyn-like' annotation. Partial and truncated transcripts were included, and their percent coverage reported (Fig. S2). Annotated transcripts with reported percent identities and coverage, when applicable, are shown in Fig. S2. A simplified version of the results is shown in Fig. 2. Annotated transcripts were cross-reference to available genomic data for further validation for *P. bracteatum* (PUWZ01), *P. armeniacum* (JAJJWX01), *P. atlanticum* (JAJJMB01), *P. californicum* (JAJJMC01), *P. nudicaule* (JAJJMA01) (Fig. S4 and Table S3). Orthogroups were identified using OrthoFinder V2.5.5[35] (Table S4).

Morphinan alkaloid profiling

High-resolution ESI-LTQ-Orbitrap-XL MS was performed as described previously[73] either (i) by direct infusion via a syringe pump or (ii) by LC performed using an Accela HPLC (Thermo Fisher; Waltham, MA) equipped with a Poroshell 120 SB-C18 column, 2.1×50 mm, 2.7 µm (Agilent Technologies; Santa Clara, CA). Direct infusion was performed in conjunction with isocratic solvent flow (50:50 Solvent A:Solvent B, 0.5 mL/min) using a T-bar union. Briefly, for each standard, a steady flow (5 µL/min) of a methanolic (100%) or partially aqueous (50:50 water:methanol) solution (1 µg/mL) was achieved using a 500-µL Hamilton syringe pump. This flow was streamed into HPLC solvent flow, followed by ESI under the following conditions: source voltage 3.00 kV, current ~100 µA, capillary temperature 380 °C, voltage 6.00 V, vaporizer temperature 400 °C, tube lens 45 V. Owing to the thermal stability of alkaloids, and their ease of ionization, the same source conditions were used in all cases. Continuous injection of alkaloid permitted opportunity to optimize MS conditions for each standard; for example, different collision energies were tried for every standard to determine best settings. To observe the retention time for each standard with our chosen HPLC-based analysis method, fractionation was performed on five microliters of alkaloid at 5 µM, injected into solvent flow (0.5 mL/min) with a gradient of Solvent A [10 mM ammonium acetate, pH 5.5, 5% (v/v) acetonitrile] and Solvent B (100% acetonitrile). Specifically, the gradient was as follows: 100–80% Solvent A over 5 min, 80–50% over 3 min, 50–0% over 3 min, isocratic at 0% for 2 min, 0–100% over 0.1 min, and isocratic at 100% for 1.9 min. The total run time was 15 min with data collected for 10 min. The ESI conditions were identical to those used for direct infusion analyzes of standards (via T-bar union and coupled HPLC flow, described above). Identical source conditions were used for the analysis of poppy extract. Following ionization, LTQ-Orbitrap-XL analysis was conducted using a parent-ion list (> 100 *m/z*) of known alkaloid masses targeted for collision-induced dissociation (CID) spectra acquisition.

AKR expression and purification

Synthetic constructs of *AKRs* were ordered from TWIST biosciences. Sequences from *P. apokrinomenon*, *P. burseri*, *P. glaucum*, *P. lasiothrix*, *P. miyabeanum*, *P. nudicaule*, *P. radicatum*, *P. rupifragium*, *P. spicatum*, and *P. triniifolium* were obtained from transcriptome analysis. *AKR* sequences from *REPI* were ordered without the fused *DRS* from *P. somniferum* and *P. bracteatum* from NCBI accession numbers KP985721 and KP985719 respectively and *P. lasiothrix*, and *P. spicatum* from transcriptomes analysis. *P. somniferum* COR (isoform 1.3) sequence was obtained from NCBI accession number AAF13738. Synthetic constructs were cloned into pET47b expression vector, recombinantly expressed using Arctic Express *E. coli* cells, and purified as previously described[29]. Starter cultures were grown overnight in 50 mL Luria–Bertani (Miller) broth supplemented with 30 mg/L kanamycin and 35 mg/L gentamycin (LBKG) at 25 °C with shaking at 170 rpm to an OD_{595} value of ~0.4, and subsequently used to inoculate 1-liter cultures using LBKG broth. Cultures were grown at 30 °C to an OD_{595} value of 0.5–0.6 and cooled to 16 °C for 30 min. Isopropyl β-D-1-thiogalactopyranoside was added to a final concentration of 1 mM to induce recombinant protein expression and cultures were incubated at 16 °C for 24 h. Cells were harvested by centrifugation and cell pellets were resuspended in lysis buffer [50 mM sodium phosphate, pH 8.0, 300 mM NaCl, 15% (v/v) glycerol]. Resuspended pellets stored at −80 °C were thawed and lysed by sonication in the presence of lysozyme and DNase, cell debris was subsequently removed by centrifugation at 4 °C. Supernatant was incubated with 1 mL of lysis buffer equilibrated TALON resin (Clontech; Kusatsu,

Japan) with shaking at 65 rpm for 45 min on ice. The resin was washed with 10 mL of lysis buffer followed by a 40 mL lysis buffer wash incubated for 45 min with shaking at 65 rpm on ice. The resin was then washed with 20 mL lysis buffer supplemented with 5 mM imidazole, followed by 2 mL lysis buffer supplemented with 10 mM imidazole, and finally recombinant protein was eluted with 4 mL of lysis buffer supplemented with 200 mM imidazole. Imidazole concentration was reduced to less than 1 mM by ultrafiltration (30k). Protein purity was determined by SDS-PAGE (Figs. S16 and S20). Protein concentration was measured by absorbance at 280 nm based on a theoretical extinction coefficient[74].

Mutagenesis

Site-directed mutagenesis was performed in the pET47b plasmid using a previously described method[75] used in our previous work[29]. Briefly, nucleotide substitutions were introduced into target codons by PCR site directed mutagenesis using Q5 High-Fidelity DNA polymerase (New England Biolabs; Ipswich, MA) and oligonucleotide primers (Integrated DNA Technologies; Coralville, IA) containing targeted substitutions[76] (Table S9). Constructs were verified by dideoxynucleotide chain-termination sequencing.

DRR enzyme assays

Reductive and oxidation enzyme assays were performed as previously described[4] with the following modifications. Reductive assays were run at 37 °C with 20 μM 1,2-dihydroreticuline, 500 μM NADPH, 100 mM Bis-tris propane, pH 7.0 in 50 μL reactions. Oxidative assays were run at 37 °C with 20 μM (*R*)-reticuline, 500 μM $NADP^+$, 100 mM Bis-tris propane, pH 8.8, in 50 μL reactions. Enzyme concentration and assay time were run within the linear range, less than 10% substrate conversion, for *Papaver* DRRs (Table S10) and *P. somniferum* DRR(REPI) mutants (Table S11). Enzymes with relatively weak DRR activity precluded proper determination of specific activity and were assayed overnight using 2 μg of recombinant protein under otherwise standard reduction or oxidation conditions. Reductive kinetic assays were performed using 500 μM NADPH and 1 μM to 80 μM 1,2-dehydroreticuline with optimized pH (100 mM Bis-tris), temperature, and assay times (Table S12). Oxidative kinetic assays were run using 500 μM $NADP^+$ and 2.5 μM to 500 μM (*R*)-reticuline with optimized pH (100 mM Bis-tris), temperature, and assay times (Table S12). Reactions were quenched with 300 μL of methanol and diluted to 1 μM total alkaloid with 650 μL of LC-MS solvent A [0.08% (v/v) acetic acid: acetonitrile (95:5)] before analysis by LC-MS as previously described[4]. Enzyme assays were performed in triplicate and analytes quantified using a five-point standard curve. For enzyme kinetics, quenching methanol was evaporated and resuspended in LC-MS solvent A. Michaelis–Menton and substrate inhibition kinetics were determined using Graphpad Prism 5 (Insight Partners, New York, NY) software.

COR enzyme assays

Reductive and oxidation in vitro enzyme assays were conducted as previously described[74], employed in our previous work[29], with the following modifications. Reductive assays were run at 25 °C with 50 μM codeinone, 1 mM NADPH, 100 mM Bis-tris propane pH 8.0 in 50 μL reactions. Oxidative assays were run at 25 °C with 50 μM codeine, 1 μM $NADP^+$, 100 mM Bis-tris propane pH 8.8 in 50 μL reactions. Enzyme concentration and assay time were run within the linear range, less than 10% substrate conversion (Table S10). Steady state enzyme kinetics were carried out for representative CORs ranging from higher to lower specific activities. Reductive kinetic assays were run with 1 mM NADPH and 1 μM to 400 μM codeinone with optimized pH (100 mM Bis-tris), temperature, and assay times (Table S12). Oxidative kinetic assays were run with 1 mM $NADP^+$ and 1 μM to 400 μM codeine with optimized pH (100 mM Bis-tris), temperature, and assay times (Table S12). Reactions were quenched with 300 μL of methanol before analysis by LC-MS as previously described[75]. Enzyme assays were performed in triplicates and analytes quantified using a five-point standard curve. For enzyme kinetics, quenching methanol was evaporated and resuspended in LC-MS solvent A (10 mM ammonium acetate, pH 5.5). Michaelis–Menton kinetic analysis were preformed using Graphpad Prism 5 software.

Transient expression of DRS, DRR, REPI, and SalSyn in yeast

Synthetic constructs of *DRS*, *DRR*, *REPI*, and *SalSyn* were ordered from Twist Biosciences (San Francisco, CA). Sequences from *P. burseri*, *P. lasiothrix*, *P. nudicaule*, *P. orientale*, *P. triniifolium*, and *P. spicatum* were obtained from transcriptome analysis. *P. rhoeas DRS* and *P. somniferum SalSyn* and *REPI* were obtained from NCBI accession numbers KP985722, EF451150 and KP985721 respectively. To avoid incorrect membrane insertion of cytochrome P450 domains the N-terminal of DRS and REPI were substituted with that of germacrene A oxidase (GAO) as previously reported[43] and SalSyn N-terminal substituted with that of cheilanthifoline synthase (CFS) as previously reported[42]. All genes were codon optimized (GenScript; Piscataway, NJ) and are shown in Table S7. For transient expression, *Papaver* DRS, DRR, REPI, and SalSyn synthetic genes were cloned into pESC-His vector under PGK1 promoter (DRS, REPI, SalSyn) and TDH3 (DRR). DRS, DRR, and SalSyn genes were transformed into the engineered yeast strain BC with chromosome integrated *P. somniferum* BIA uptake permease 1 (BUP1) and CYP reductase 2 (CPR2). REPI and unfused DRS-DRR genes were transformed into the strain BC with an integrated *P. somniferum* SalSyn, strain BCSS, used to distinguish between (*S*)- and (*R*)-reticuline by conversion of (*R*)-reticuline to salutaridine. All transformations were preformed using the LiAc/PEG/single-stranded carrier DNA (ssDNA) method[77]. Chromosomal integration of BUP1, CRP2, and SalSyn were engineered from the CEN.PK parent strain using CRISPR-Cas9 technology[78].

Yeast substrate feeding

Three colonies from transformed strain BC or BCSS were used to inoculate 500 μL SD-his medium starter cultures grown overnight at 30 °C and 900 rpm using a gyratory microplate shaker. Feeding experiments were carried out by inoculating 200 μL of fresh SD-His medium containing 50 μM of substrate with 10 μL of starter culture and subsequently grown for 12, 24, or 48 h. Reactions were quenched by adding two volumes of acetonitrile and centrifuged for 30 min at 2000*g*. Supernatants were then analyzed by LCMS using the same protocol as for COR assays and analytes were quantified using five-point standard curves.

Modeling of DRR and COR structures

Homology models of *P. somniferum* DRR(REPI), *P. miyabeanum* DRR2, and *P. burseri* DRR were prepared with Modeller[79] using *P. somniferum* COR as a template (PDB: 7MBF). Induced-fit substrate and cofactor docking were preformed using Molecular Operating Environment (MOE) (https://www.chemcomp.com/products.htm). Standard default docking settings were used. *P. somniferum* COR coordinates (PDB: 7MBF) were used in docking studies. PyMOL was used to visualize AKR models (https://pymol.org/2/).

Statistics and Reproducibility

Error bars in all figures correspond to the mean ± standard deviation of three independent biological replicates.

Reporting summary

Further information on research design is available in the Nature Portfolio Reporting Summary linked to this article.

Data availability

Data used to plot all graphs is available as Supplementary Data 1. All other data are available from the corresponding author on reasonable request. Other supplementary data is available in the Supplementary Information file. Raw nucleotide sequence data have been deposited in the National Center for Biotechnology Information (NCBI) Short Read Archive (SRA) database under the following accession codes: SRR27145420, SRR27235872,

SRR27235873, SRR27235874, SRR27235875, SRR27212614, SRR27212567, SRR27212568, SRR27212569, SRR27283754, SRR27283755, and SRR27283756 under the bioproject PRJNA1050196. Assembled transcriptomes have been deposited in the NCBI Transcriptome Shotgun Assembly (TSA) database under the following accession codes: GKSI00000000, GKSF00000000, GKSE00000000, GKSG00000000, GKSD00000000, GKSB00000000, GKSA00000000, GKRY00000000, GKRX00000000, GKRW00000000, GKRV00000000, GKRS00000000 under the bioproject PRJNA1050196. Nucleotide sequence data have been deposited in the NCBI Genbank database under the following accession codes: *AKRs* (OR829681, OR829682, OR829683, OR829684, OR829685, OR829686, OR829687, OR829688, OR829689, OR829690, OR829691, OR829692, OR829693, OR829694, OR829695, OR829696, OR829697, OR829698, OR29699); *DRS-AKR* fusions (OR829700, OR829701); *DRSs* (OR838695, OR838696, OR838697); and *SalSyns* (OR829703, OR829702, OR838698).

Received: 15 April 2024; Accepted: 18 October 2024;
Published online: 29 October 2024

References

1. Dastmalchi, M., Park, M. R., Morris, J. S. & Facchini, P. Family portraits: the enzymes behind benzylisoquinoline alkaloid diversity. *Phytochem. Rev.* **17**, 249–277 (2018).
2. World Health Organization. World health organization model list of essential medicines. *Ment. Holist. Health.: Some Int. Perspect.* **21**, 119–134 (2019).
3. Board, I. N. C. Narcotic Drugs - Technical Report. (2019).
4. Farrow, S. C., Hagel, J. M., Beaudoin, G. A. W., Burns, D. C. & Facchini, P. J. Stereochemical inversion of (*S*)-reticuline by a cytochrome P450 fusion in opium poppy. *Nat. Chem. Biol.* **11**, 728–732 (2015).
5. Winzer, T. et al. Morphinan biosynthesis in opium poppy requires a P450-oxidoreductase fusion protein. *Science* **349**, 309–312 (2015).
6. Gesell, A. et al. CYP719B1 is salutaridine synthase, the C-C phenol-coupling enzyme of morphine biosynthesis in opium poppy. *J. Biol. Chem.* **284**, 24432–24442 (2009).
7. Lenz, R. & Zenk, M. H. Purification and properties of codeinone reductase (NADPH) from *Papaver somniferum* cell cultures and differentiated plants. *Eur. J. Biochem.* **233**, 132–139 (1995).
8. Ziegler, J. et al. Comparative transcript and alkaloid profiling in *Papaver* species identifies a short chain dehydrogenase/reductase involved in morphine biosynthesis. *Plant J.* **48**, 177–192 (2006).
9. Dastmalchi, M. et al. Neopinone isomerase is involved in codeine and morphine biosynthesis in opium poppy. *Nat. Chem. Biol.* **15**, 384–390 (2019).
10. Chen, X. et al. A pathogenesis-related 10 protein catalyzes the final step in thebaine biosynthesis. *Nat. Chem. Biol.* **14**, 738–743 (2018).
11. Hagel, J. M. & Facchini, P. J. Dioxygenases catalyze the *O*-demethylation steps of morphine biosynthesis in opium poppy. *Nat. Chem. Biol.* **6**, 273–275 (2010).
12. Grothe, T., Lenz, R. & Kutchan, T. M. Molecular characterization of the salutaridinol 7-*O*-acetyltransferase involved in ormphine biosynthesis in opium poppy *Papaver somniferum*. *J. Biol. Chem.* **276**, 30717–30723 (2001).
13. Li, Y., Winzer, T., He, Z. & Graham, I. A. Over 100 million years of enzyme evolution underpinning the production of morphine in the Papaveraceae family of flowering plants. *Plant Commun.* **1**, 100029 (2020).
14. Yang, X. et al. Three chromosome-scale *Papaver* genomes reveal punctuated patchwork evolution of the morphinan and noscapine biosynthesis pathway. *Nat. Commun.* **12**, 6030 (2021).
15. Catania, T. et al. A functionally conserved STORR gene fusion in *Papaver* species that diverged 16.8 million years ago. *Nat. Commun.* **13**, 3150 (2022).
16. Zhang, R.-G. et al. Subgenome-aware analyses suggest a reticulate allopolyploidization origin in three *Papaver* genomes. *Nat. Commun.* **14**, 2204 (2023).
17. Jensen, R. A. Enzyme recruitment in evolution of new function. *Annu. Rev. Microbiol.* **30**, 409–425 (1976).
18. Yčas, M. On earlier states of biochemical systems. *J. Theor. Biol.* **44**, 145–160 (1974).
19. Huang, R., O'Donnell, A. J., Barboline, J. J. & Barkman, T. J. Convergent evolution of caffeine in plants by co-option of exapted ancestral enzymes. *Proc. Natl Acad. Sci. USA* **113**, 10613–10618 (2016).
20. Rieseberg, T. P. et al. Crossroads in the evolution of plant specialized metabolism. *Sem. Cell Devel. Biol.* **134**, 37–58 (2023).
21. Khersonsky, O., Roodveldt, C. & Tawfik, D. Enzyme promiscuity: evolutionary and mechanistic aspects. *Curr. Opin. Chem. Biol.* **10**, 498–508 (2006).
22. D'Ari, R. & Casadesús, J. Underground metabolsim. *Bioessays* **20**, 181–186 (1998).
23. Penning, T. M. The aldo-keto reductases (AKRs): Overview. *Chem. -Biol. Interact.* **234**, 236–246 (2015).
24. Welle, R. & Grisebach, H. Isolation of a novel NADPH-dependent reductase which coacts with chalcone synthase in the biosynthesis of 6′-deoxychalcone. *FEBS Lett.* **236**, 221–225 (1988).
25. Jirschitzka, J. et al. Plant tropane alkaloid biosynthesis evolved independently in the Solanaceae and Erythroxylaceae. *Proc. Natl Acad. Sci. USA* **109**, 10304–10309 (2012).
26. De-Eknamkul, W. & Zenk, M. H. Purification of properties of 1,2-dehydroreticuline reductase from *Papaver somnifer*um seedlings. *Phytochemisty* **31**, 813–821 (1992).
27. Di Costanzo, L., Drury, J. E., Christianson, D. W. & Penning, T. M. Structure and catalytic mechanism of human steroid 5β-reductase (AKR1D1). *Mol. Cell. Endocrinol.* **301**, 191–198 (2009).
28. Schlegel, B. P., Ratnam, K. & Penning, T. M. Retention of NADPH-linked quinone reductase activity in an aldo-keto reductase following mutation of the catalytic tyrosine. *Biochemistry* **37**, 11003–11011 (1998).
29. Carr, S. C., Torres, M. A., Morris, J. S., Facchini, P. J. & Ng, K. K. S. Structural studies of codeinone reductase reveal novel insights into aldo-keto reductase function in benzylisoquinoline alkaloid biosynthesis. *J. Biol. Chem.* **297**, 101211 (2021).
30. Sariyar, G. Biodiversity in the alkaloids of Turkish *Papaver* species. *Pure Appl. Chem.* **74**, 557–574 (2002).
31. One Thousand Plant Transcriptomes Initiative. One thousand plant transcriptomes and the phylogenomics of green plants. *Nature* **574**, 679–685 (2019).
32. Carpenter, E. J. et al. Access to RNA-sequencing data from 1,173 plant species: The 1000 Plant transcriptomes initiative (1KP). *GigaScience* **8**, giz126 (2019).
33. Loza-Muller, L., Shitan, N., Yamada, Y. & Vázquez-Flota, F. AmABCB1, an alkaloid transporter from seeds of *Argemone mexicana* L (Papaveraceae). *Planta* **254**, 122 (2021).
34. Mazuecos-Aguilera, I. & Suárez-Santiago, V. N. Identification of candidate genes involved in the determinism of pollen grain aperture morphology by comparative transcriptome analysis in Papaveraceae. *Plants* **12**, 1570 (2023).
35. Emms, D. M. & Kelly, S. OrthoFinder: phylogenetic orthology inference for comparative genomics. *Genome Biol.* **20**, 238 (2019).
36. Farrow, S. C. & Facchini, P. J. Dioxygenases catalyze *O*-demethylation and *O*,*O*-demethylenation with widespread roles in benzylisoquinoline alkaloid metabolism in opium poppy. *J. Biol. Chem.* **288**, 28997–29012 (2013).
37. Pourmazaheri, H. et al. Comparative analysis of the root and leaf transcriptomes in *Chelidonium majus* L. *PLoS ONE* **14**, e0215165 (2019).
38. Liao, D. et al. Identification and developmental expression profiling of putative alkaloid biosynthetic genes in *Corydalis yanhusuo* bulbs. *Sci. Rep.* **6**, 19460 (2016).

39. Xu, D. et al. Integration of full-length transcriptomics and targeted metabolomics to identify benzylisoquinoline alkaloid biosynthetic genes in *Corydalis yanhusuo*. *Hort. Res.* **8**, 16 (2021).
40. Jez, J. M., Bennett, M. J., Schlegel, B. P., Lewis, M. & Penning, T. M. Comparative anatomy of the aldo–keto reductase superfamily. *Biochem. J.* **326**, 625–636 (1997).
41. Diaz-Bárcena, A., Fernandez-Pacios, L. & Giraldo, P. Structural characterization and molecular dynamics study of the REPI fusion protein from *Papaver somniferum* L. *Biomolecules* **14**, 2 (2023).
42. Galanie, S., Thodey, K., Trenchard, I. J., Filsinger Interrante, M. & Smolke, C. D. Complete biosynthesis of opioids in yeast. *Science* **349**, 1095–1100 (2015).
43. Fossati, E. et al. Reconstitution of a 10-gene pathway for synthesis of the plant alkaloid dihydrosanguinarine in *Saccharomyces cerevisiae*. *Nat. Commun.* **5**, 3283 (2014).
44. Liscombe, D. K., MacLeod, B. P., Loukanina, N., Nandi, O. I. & Facchini, P. J. Evidence for the monophyletic evolution of benzylisoquinoline alkaloid biosynthesis in angiosperms. *Phytochemistry* **66**, 1374–1393 (2005).
45. Ziegler, J. et al. Evolution of morphine biosynthesis in opium poppy. *Phytochemistry* **70**, 1696–1707 (2009).
46. Ober, D. & Hartmann, T. Homospermidine synthase, the first pathway-specific enzyme of pyrrolizidine alkaloid biosynthesis, evolved from deoxyhypusine synthase. *Proc. Natl Acad. Sci. USA* **96**, 14777–14782 (1999).
47. Ozber, N. et al. Alkaloid binding to opium poppy major latex proteins triggers structural modification and functional aggregation. *Nat. Commun.* **13**, 6768 (2022).
48. Clifton, B. E. et al. Evolution of cyclohexadienyl dehydratase from an ancestral solute-binding protein. *Nat. Chem. Biol.* **14**, 542–547 (2018).
49. Kaltenbach, M. et al. Evolution of chalcone isomerase from a noncatalytic ancestor. *Nat. Chem. Biol.* **14**, 548–555 (2018).
50. Méteignier, L.-V., Nützmann, H.-W., Papon, N., Osbourn, A. & Courdavault, V. Emerging mechanistic insights into the regulation of specialized metabolism in plants. *Nat. Plants* **9**, 22–30 (2022).
51. Jia, Y. et al. The tissue-specific chromatin accessibility landscape of *Papaver somniferum*. *Front. Genet.* **14**, 1136736 (2023).
52. Xu, Y. et al. Evolutionary analysis of conserved non-coding elements subsequent to whole-genome duplication in opium poppy. *Plant J.* **116**, 1804–1824 (2023).
53. Kajikawa, M. et al. Genomic insights into the evolution of the nicotine biosynthesis pathway in tobacco. *Plant Physiol.* **174**, 999–1011 (2017).
54. Xu, S. et al. Wild tobacco genomes reveal the evolution of nicotine biosynthesis. *Proc. Natl Acad. Sci. USA* **114**, 6133–6138 (2017).
55. Schrittwieser, J. H., Velikogne, S. & Kroutil, W. Biocatalytic imine reduction and reductive amination of ketones. *Adv. Synth. Catal.* **357**, 1655–1685 (2015).
56. Langley, C. et al. Expansion of the catalytic repertoire of alcohol dehydrogenases in plant metabolism. *Angew. Chem.* **61**, e202210934 (2022).
57. Hong, B. et al. Biosynthesis of strychnine. *Nature* **607**, 617–622 (2022).
58. Schotte, C. et al. Directed biosynthesis of mitragynine stereoisomers. *J. Am. Chem. Soc.* **145**, 4957–4963 (2023).
59. Stavrinides, A. et al. Structural investigation of heteroyohimbine alkaloid synthesis reveals active site elements that control stereoselectivity. *Nat. Commun.* **7**, 12116 (2016).
60. Mangas-Sanchez, J. et al. Imine reductases (IREDs). *Curr. Opin. Chem. Biol.* **37**, 19–25 (2017).
61. Wu, K., Huang, J. & Shao, L. Imine reductases: Multifunctional biocatalysts with varying active sites and catalytic mechanisms. *ChemCatChem* **14**, e202200921 (2022).
62. Czekster, C. M., Vandemeulebroucke, A. & Blanchard, J. S. Kinetic and chemical mechanism of the dihydrofolate reductase from *Mycobacterium tuberculosis*. *Biochemistry* **50**, 367–375 (2011).
63. Meneely, K. M. & Lamb, A. L. Two structures of a thiazolinyl imine reductase from *Yersinia enterocolitica* provide insight into catalysis and binding to the nonribosomal peptide synthetase module of HMWP1. *Biochemistry* **51**, 9002–9013 (2012).
64. Rodríguez-Mata, M. et al. Structure and activity of NADPH-dependent reductase Q1EQE0 from *Streptomyces kanamyceticus*, which catalyses the (*R*)-selective reduction of an imine substrate. *ChemBioChem* **14**, 1372–1379 (2013).
65. He, X. & Brossi, A. 1,2-dehydroreticuline: Conversion of iminium salts into enamines. *J. Nat. Prod.* **56**, 973–975 (1993).
66. Battersby, A. R., Foulkes, D. M., Hirst, M., Parry, G. V. & Staunton, J. Alkaloid Biosynthesis. Part X1. Studies related to the formation and oxidation of reticuline in morphine biosynthesis. *L. Chem Soc. C* 210–216 (1968).
67. Leong, B. J. & Last, R. L. Promiscuity, impersonation and accommodation: evolution of plant specialized metabolism. *Curr. Opin. Struct. Biol.* **47**, 105–112 (2017).
68. He, Y. et al. Structural and functional evolution of isopropylmalate dehydrogenases in the leucine and glucosinolate pathways of *Arabidopsis thaliana*. *J. Biol. Chem.* **286**, 28794–28801 (2011).
69. Fan, P. et al. In vitro reconstruction and analysis of evolutionary variation of the tomato acylsucrose metabolic network. *Proc. Natl. Acad. Sci. USA* **113**, E239–48(2016).
70. Krishnamurthy, P., Pothiraj, R., Suthanthiram, B., Somasundaram, S. M. & Subbaraya, U. Phylogenomic classification and synteny network analyses deciphered the evolutionary landscape of aldo–keto reductase (AKR) gene superfamily in the plant kingdom. *Gene* **816**, 146169 (2022).
71. Guo, L. et al. The opium poppy genome and morphinan production. *Science* **362**, 343–347 (2018).
72. Gambino, G., Perrone, I. & Gribaudo, I. A Rapid and affective method for RNA extraction from different tissues of grapevine and other woody plants. *Phytochem. Anal.* **19**, 520–525 (2008).
73. Perdomo-Menéndez, I. M., Hagel, J. M. & Facchini, P. J. Benzylisoquinoline alkaloid analysis using high-resolution Orbitrap LC-MS^n. *J. Mass Spectrom.* **56**, e4683 (2020).
74. Gill, S. C. & von Hippel, P. H. Calculation of protein extinction coefficients from amino acid sequence data. *Anal. Biochem.* **182**, 319–326 (1989).
75. Dastmalchi, M., Chang, L., Torres, M. A., Ng, K. K. S. & Facchini, P. J. Codeinone reductase isoforms with differential stability, efficiency and product selectivity in opium poppy. *Plant J.* **95**, 631–647 (2018).
76. Zheng, L. An efficient one-step site-directed and site-saturation mutagenesis protocol. *Nucleic Acids Res.* **32**, e115 (2004).
77. Gietz, R. D. & Schiestl, R. H. Frozen competent yeast cells that can be transformed with high efficiency using the LiAc/SS carrier DNA/PEG method. *Nat. Protoc.* **2**, 1–4 (2007).
78. Jensen, N. B. et al. EasyClone: method for iterative chromosomal integration of multiple genes *Saccharomyces cerevisiae*. *FEMS Yeast Res.* **14**, 238–248 (2014).
79. Webb, B. & Sali, A. Comparative protein structure modeling using MODELLER. *Curr. Protoc. Bioinform.* **54**, 5.6.1–5.6.37 (2016).
80. Carolan, J. C., Hook, I. L. I., Chase, M. W., Kadereit, J. W. & Hodkinson, T. R. Phylogenetics of *Papaver* and related genera based on DNA sequences from ITS nuclear ribosomal DNA and plastid *trnL* intron and *trnL–F* intergenic spacers. *Ann. Bot.* **98**, 141–155 (2006).
81. Madeira, F. et al. Search and sequence analysis tools services from EMBL-EBI in 2022. *Nucleic Acids Res.* **50**, W276–W279 (2022).
82. The PyMOL Molecular Graphics System, Version 2.2.2 Schrödinger, LLC.

Acknowledgements

This work was funded by an Alberta Innovates Strategic Research Project grant, and by Natural Sciences and Engineering Research Council of Canada Discovery grants to P.J.F. and K.K.S.N.

Author contributions

S.C.C. designed the experiments, acquired and analyzed data, and wrote the manuscript. F.R. acquired and analyzed data. X.C. and J.M.H. performed the transcriptomics and metabolomics, respectively. K.K.S.N. reviewed the manuscript. P.J.F. conceived the study, supervised the research, revised the manuscript, and approved it for submission.

Competing interests

The authors declare no competing interests.

Additional information

Supplementary information The online version contains supplementary material available at https://doi.org/10.1038/s42003-024-07100-w.

Correspondence and requests for materials should be addressed to Peter J. Facchini.

Peer review information *Communications Biology* thanks the anonymous reviewers for their contribution to the peer review of this work. Primary Handling Editors: Huijuan Guo and David Favero. A peer review file is available.